NOTE TO USERS

Passive Earth Pressure on Embedded Plate Anchors in Sand

Farhana Rahman

A Thesis

In

The Department

Of

Building, Civil and Environmental Engineering

Presented in Partial Fulfillment of the Requirements

For the Degree of Masters of Applied Science at

Concordia University

Montreal, Quebec, Canada

September 2005

Your file Votre référence
ISBN: 0-494-10229-2
Our file Notre référence
ISBN: 0-494-10229-2

ABSTRACT

Earth pressure on anchor plates is considered a viable resisting force for the design of underground structures. The theories available in the literature overestimate the earth pressure on these anchors, leading to unsafe design and perhaps loss of structures and lives.

The present investigation is directed to study the passive earth pressure distribution as function of the stress history of the soil represented in terms of the overconsolidation ratio and the depth of embedment. The objective of this study is to validate the theories of Hanna and Khoury (2005) and to examine the case of earth pressures acting on anchor plate, which believed to receive little attention in the literature. Numerical models were developed using the finite element technique and the constitutive laws of Mohr-Coulomb for cases of retaining walls and embedded anchor plate in sand.

The produced results reconfirmed the theories developed by Hanna and Khoury (2005) for the cases of walls retaining overconsolidated sand and walls retaining overconsolidated backfill overlying natural deposit. In addition, the results showed that the earth pressure on anchor plates increases due to the increase of the angle of shearing resistance and the overconsolidation ratio of the sand. Furthermore, the deduced values of the earth pressure are significantly lower than those predicted by the classic theories of earth pressures. This was due to the fact that the effect of the depth of embedment was ignored in developing theories.

Design theories were developed for the case of anchor plate retaining overconsolidated sand for the ultimate load and the allowable displacement conditions.

ACKNOWLEDGEMENTS

At first, I would like to pay my outmost respect to Almighty Allah, for granting me this wonderful opportunity to work and to live

I would like to avail this opportunity to express my sincere gratitude to Professor Dr. A. M. Hanna for his overall supervision, invaluable suggestions and constant encouragement at all stages of the present works. Starting from the elementary concepts, it is his keen interest and ardent inspiration that helped me to understand the topic and carried out this research work. I am honored to carry out the present study under his direct supervision.

I acknowledge the fact that the development and compilation of this research was a team effort and I am particularly grateful to Dr. Tahar Ayadat for his guidance and support through out the research. I would also like to thank Mr. Mohab Sabry and Mr. Mohammed Etezad for their assistance during the development of the numerical model.

I wish to express my sincere respect and gratitude to my parents for their understanding, patience and blessings that helped me to be what I am today.

TABLE OF CONTENTS

LIST OF SYMBOLS

SYMBOL	REPRESENTS
A	Area of the plate material
c	Cohesion
CPT	Cone penetration test
D	Depth of embedment of anchor plate
D_r	Relative density
d_{eq}	Equivalent thickness of the plate material
E	Young's modulus of soil
E_c	Young's modulus of concrete
E_s	Young's modulus of steel
e_y	Eccentricity
EA	Axial stiffness
EI	Flexural rigidity
H_{CG}	Location of center of gravity from the top of the anchor plate
H	Height of the retaining wall
h_a	Height of the anchor plate
I	Moment of inertia
K_p	Coefficient of passive earth pressure
K_o'	Effective coefficient of earth pressure at rest
K_o	Coefficient of earth pressure at rest
$K_{o(NC)}$	Coefficient of earth pressure at rest for normally consolidated soil
$K_{o(OC)}$	Coefficient of earth pressure at rest for overconsolidated soil
$K_{p(NC)}$	Coefficient of passive earth pressure for normally consolidated soil

$K_{p(OC)}$	Coefficient of passive earth pressure for over consolidated soil
K	Dimensionless modulus number
l_e	Average element size in finite element mesh
n_c	Global coarseness number
n	Exponent
OCR	Overconsolidation ratio
P_a	Atmospheric pressure
P_{rm}	Modified total earth pressure for overconsolidated sand (δ=0)
P_w	Pore water pressure
P_{ult}	Ultimate load
R_{inter}	Strength reduction factor
R	Reduction factor
W	Weight of the plate material
w	Weight of the given slice
μ	Poisson's ratio
ψ	Angle of Dilatancy
Δ	Displacement
ϕ	Angle of shearing resistance
λ	Rotational angle of vertical anchor plate
δ	Angle of wall soil friction
α	Empirical coefficient
τ	Shear strength of soil
σ_1	Major principle effective stress
σ_3	Minor principle effective stress
σ_h	Horizontal effective stress
σ_v	Vertical effective stress

LIST OF TABLES

LIST OF FIGURES

CHAPTER 1

INTRODUCTION

1.1 Preface

Earth pressure theories are integral part in developing design theories for foundation engineering. Furthermore, earth-retaining structures such as retaining walls, bridge abutments, reinforced concrete culverts, sheet piles, and earth anchors are designed solely to sustain earth pressures. Thus earth pressure theories occupy a paramount position in the field of geotechnical engineering.

Compaction, in general, is the densification of soil by removal of air from voids, which requires mechanical energy in the form of compaction effort. In the construction of retaining wall structures, loose soil must be compacted to increase its strength characteristics. During compaction, both horizontal and vertical stresses undergo a complex stress increase; these stresses remain locked-in after removing the load, causing the soil to consolidate. Design of these structures must consider the level of overconsolidation achieved during compaction. In other words, the effect of consolidation process should be incorporated in the development of theories of earth pressures.

While the prediction of the active earth pressure on these structures has been well developed, the passive earth pressures on these walls as well as anchors remained lagging behind. This is due to the fact that active pressure is regarded as disturbing force, while the passive one is a resisting force, accordingly received less attention. The current design

practice ignores the effect of the presence of layered soil that frequently found in field, the depth of embedment over the anchor plate, rotation of plate anchor embedded in backfill material and the change of the overconsolidation level in the soil; as a result of the compaction process.

In the literature, several theoretical and experimental investigations can be found dealing with the magnitude and distribution of passive earth pressure behind a retaining wall. While some reports dealt with the effect of the overconsolidation, no reports were found to address the effect of internal relation between the overconsolidation and elastic parameters of soil such as soil modulus of elasticity. Furthermore, no attempts were made to investigate the magnitude and the distribution of the passive earth pressure on earth anchor conjugated with a retaining wall and embedded in homogeneous and overconsolidated backfill. Accordingly, it can be reported herein that the existing theories sometimes are overestimating these design loads acting on the embedded anchor plate in passive condition, leading to failure and loss of structures and lives.

CHAPTER 2

LITERATURE REVIEW

2.1 General

Lateral earth pressures acting on walls were one of the first soil structure interaction problem considered in the field of geotechnical engineering. The existing theories for estimating these pressures and deformations will be reviewed in this chapter. These theories and the shortcomings in their analytical capabilities are summarized here so that it could warrant further research on the subject.

2.2 Review of the Previous Theories and Analytical Procedures

Coulomb (1776) proposed a mathematical solution to calculate the earth pressure behind a retaining wall by considering the wall soil friction angle δ. The major assumption was that the failure surface was a plane surface where the friction forces are uniformly distributed and soil is isotropic and homogeneous. Thus he postulated the so-called Coulomb's Law as follows:

$$P_p = \frac{1}{2}\gamma H^2 K_p \quad \text{(2.1)}$$

Where

$$K_p = \frac{1}{\cos\delta} \times \left(\frac{1}{\left(1/\cos\delta\right) - \left(\tan^2\varphi + \tan\varphi\tan\delta\right)^{0.5}} \right)^2 \quad \text{(2.2)}$$

Rankine (1875) suggested a mathematical solution considering the plastic equilibrium condition of earth mass. He used the failure condition defied by the Mohr-Coulomb criterion of the soil to derive a passive earth pressure behind a retaining walls where δ=0. The solution is as follows:

$$K_p = \tan^2(45^0 + \frac{\varphi}{2}) \quad \ldots\ldots\ldots\ldots\ldots\ldots\ldots\ldots\ldots\ldots\ldots\ldots\ldots\ldots \quad (2.3)$$

Caquot and Kerisel (1948) introduced a solution for the passive earth pressure acting on the face of a wall. They showed a mobilized value of the wall friction angle δ depends on the type of wall movement and proposed design charts for the values of passive earth pressure coefficient (K_p). Curved failure surface for granular soil (c=0) for the case of $\varphi = \delta$. was used to generate those charts.

Rowe (1954) proposed a stress-strain theory to calculate the lateral earth pressure exerted on structures by cohesionless soils. His work was based on the calculation of earth pressures for conditions of wall deflection intermediate between at-rest and fully active or fully passive conditions.

Rowe's stress-strain theory for calculating the lateral earth pressures of soil was based on the following hypotheses:

1. The degree of orientation of soil friction angle ϕ and the wall friction angle δ depends on the degree of interlocking of the soil grains. Finally this orientation depends on the fractional movement of the shear planes or slip strains.
2. Earth pressure acting on the structure may be calculated by using conventional limit equilibrium method implementing the soil frictional angle ϕ and soil-wall friction angle δ.

He finally postulated the pressure coefficient as:

$$Ko' = Ko(1 + ho/h) \text{ ; Where } Ko' \leq Kp \ldots\ldots\ldots\ldots\ldots\ldots\ldots\ldots (2.4)$$

It is quite noticeable that there is a similarity between Rowe's early equations for compaction induced lateral earth pressure and Schmidt's (1967) later equation, which explains residual lateral earth pressure at rest resulting from overconsolidation. Schmidt's equation, which empirically allows some degree of relaxation for lateral stresses due to surcharge removal, can be expressed as:

$$Ko' = Ko(1 + ho/h)^{\alpha} \ldots\ldots\ldots\ldots\ldots\ldots\ldots\ldots\ldots\ldots\ldots\ldots (2.5)$$

Where $\alpha = 0.3$ to 0.5 for most sands

$\alpha = 1.2 \sin\phi$ for initially normally consolidated clay.

Rowe's equation basically provided an idea about compaction in terms of overconsolidation, which can affect the stress history of a soil mass. Further, a more comprehensive theory regarding compaction induced earth pressures proposed by Broms (1971).

Sowers et al (1957) proposed a theory regarding the residual lateral earth pressures induced by compaction considering the sliding planes within the soil mass and also strain reversal. They defined the compaction as the movement that takes place between the individual soil particles over one another. After performing a series of field and laboratory tests, they were able to draw a conclusion that:

1. Residual lateral pressures are of importance primarily when the structure does not deform sufficiently to establish the active earth pressure condition.
2. The residual lateral earth pressure is a function of the vertical pressure remaining on the soil after compaction.

This theory did not provide good qualitative agreement with field and laboratory data available in this field which made the theory more conservative.

Broms (1971) proposed a widely accepted stress path theory to explain the residual lateral earth pressures on rigid, vertical and non-yielding structures. This residual lateral pressure can be resulted either from compaction or other surcharge loading which is subsequently removed.

The theoretical basis of this hypothesis is illustrated in figure 2.1. The idealized stress path proposed by Broms showed a good agreement with the earlier hypothesis of Rowe (1954). According to the Broms theory, the stress relaxation with unloading is negligible until some limiting condition is reached and this limiting condition was presented by the K_1-line explained in figure 2.1.

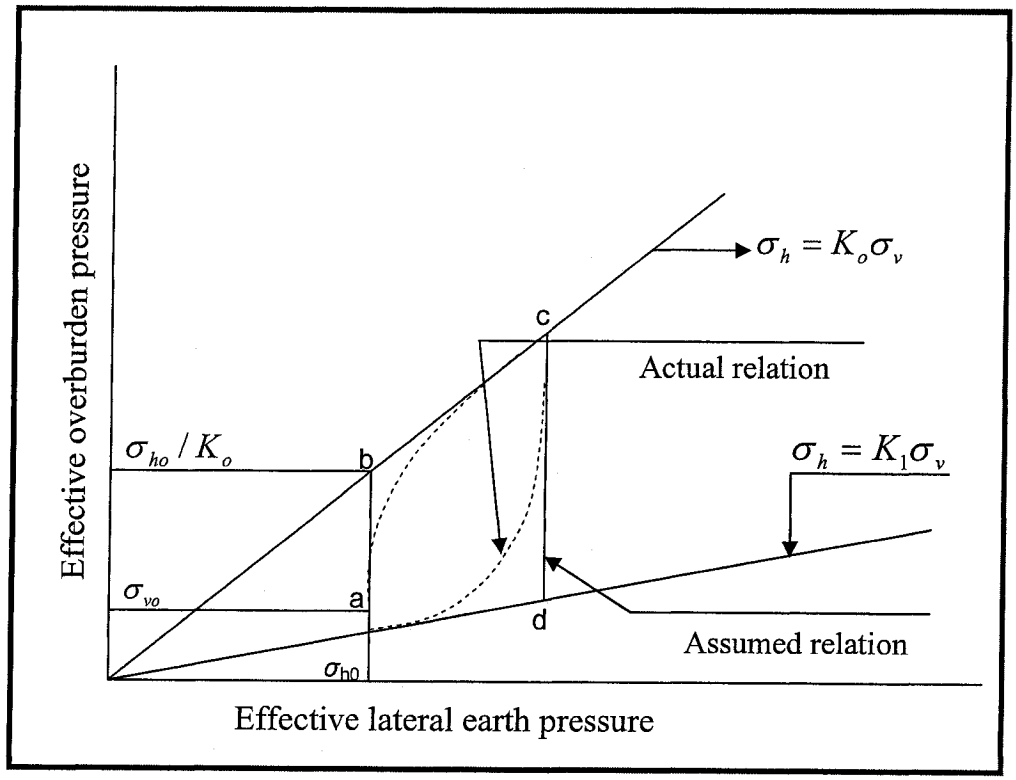

Figure 2.1 Hypothetical stress path during compaction according to Broms theory (1971)

By following this type of stress path, an element of soil can be brought to a final state. This state is represented by an effective coefficient of lateral earth pressure varying between $K_0 \leq K_{eff} \leq K_1$. Having made this idealized assumption, Broms then proposed the actual stress path followed by a real soil element which might be represented by the dashed line in figure 2.1.

A considerable body of data was available regarding K_O. For virgin loading, the normally consolidated soil reliably expressed by Jacky's (1944) equation:

$$K_O = 1 - \sin\phi \quad \ldots\ldots\ldots\ldots\ldots\ldots\ldots\ldots\ldots\ldots\ldots\ldots\ldots\ldots \quad (2.6)$$

Nevertheless, little reliable data were available to evaluate the value of K_1. To evaluate

the value of K_1, it was suggested by the Rowe (1954) as well as Ingold (1979) that $K_1 = K_P$ while Carder et al. (1977) postulated that the $K_1 = {}^{1}/_{K_O}$.

Implementation of this theory to estimate the lateral earth pressure exerted on a vertical, rigid wall by a compacted fill, Broms considered the compaction plant to represent the load applied to the fill surface. He approximated the induced vertical stresses as twice of those calculated by the Boussinesq (1885) stress equations for the infinite half-space. Figure 2.2 (a) and (b) shows the loading path for the shallow ($z < z_c$) and deep ($z > z_c$) soil element.

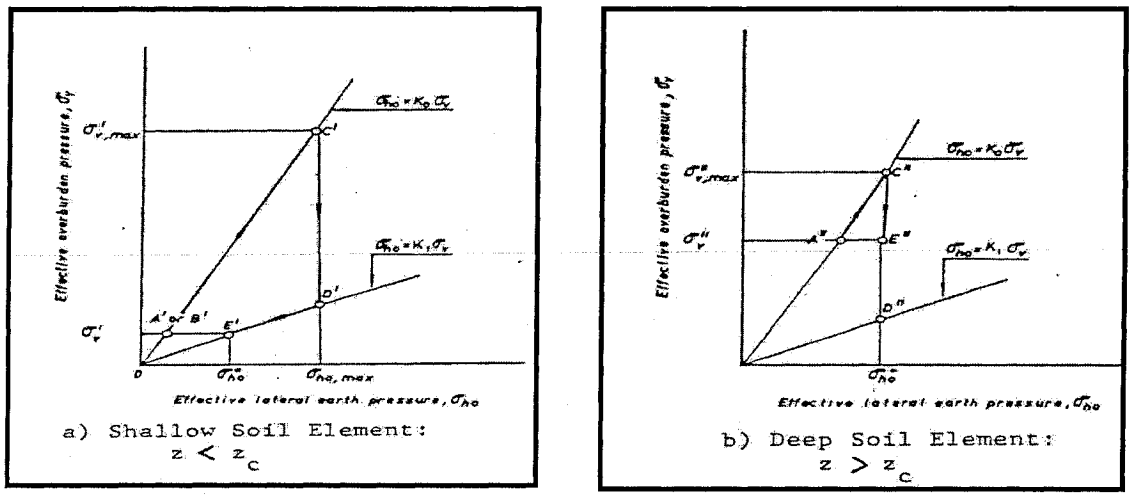

Figure 2.2 Hypothetical stress paths of shallow and deep soil element (Broms, 1971)

Broms then incorporated the single layer into multiple layers and generalized the residual lateral earth pressure distribution. His theory for calculation of residual lateral earth pressures was the first to provide a fair agreement with field observations. But it makes the value conservative in the following cases:

1. The peak lateral earth pressure acting against a wall as a result of surfacial loading can be calculated by $\sigma_h' = K_0 * \sigma_v'$ which is correct only when the surfacial

loading is of infinite lateral extent. But surface loading of an area of finite lateral extant, such as a real compaction plate, the vertical and horizontal pressures are not directly and simply related to K_0. Thus, they may not generate correct result.

2. The assumption that reloading causes negligible increases in the lateral earth pressure until the K_0-line is reached is questionable. This assumption may not be true for the calculation of earth pressure with respect to compaction as well as for overburden pressure resulting from the backfill behind a retaining wall.
3. Again, the assumption that unloading causes a negligible decrease in lateral earth pressure until the limiting condition (K_1) is reached is highly over conservative.

Broms recognized the shortcomings given in items (2) and (3) above and thus suggested the hypothetical stress path illustrated by the dashed line in figure.2.1 but did not make an attempt to quantify this type of stress path.

Ingold (1979) extended Broms theory to cases where wall deflections during backfilling were sufficient to produce an active condition in the lower layers of a backfill. The backfill was deposited or being compacted by assuming the virgin loading path $\sigma_h' = K_A * \sigma_v'$ instead of Broms $\sigma_h' = K_0 * \sigma_v'$. In addition he proposed that passive failure controlled the limiting condition, $K_1 = K_p$. Figure 2.3 shows the proposed stress path for active state condition.

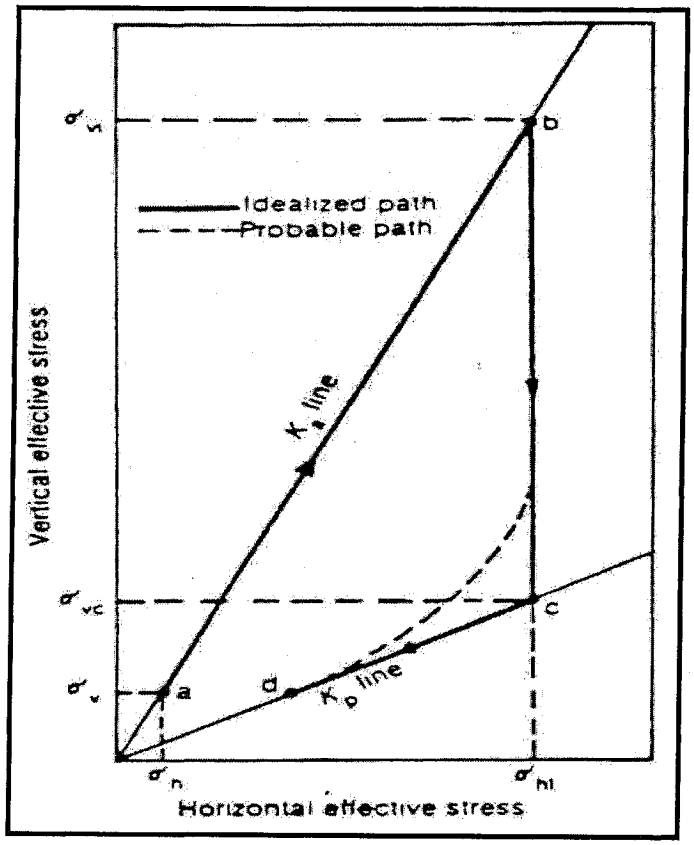

Figure 2.3 Typical stress path for active case according to Ingold (1979)

Broms original theory is applicable only to rigid, non-deflecting wall while Ingold attempted to extend for the case of deflecting wall. It might have provided a reliable lower-bound solution if Broms calculation of lateral stresses by $\sigma_h' = K_0 * \sigma_v'$ had been correct. As it is still questionable, Ingold's extension may not provide a reliable means of estimating residual compaction-induced pressures acting against deflecting structures.

Aggour and Brown (1974) were the first to attempt to model the compaction induced lateral earth pressure by means of two dimensional finite element analyses. They developed a finite element algorithm for estimating lateral earth pressures on a wall. This pressure could deflect during incremental placement and compaction of backfill in lifts without considering friction between the soil and wall.

They conducted the analysis for two different setups. At first they considered the multiple soil layer behind a retaining wall compacted at each layer. They concluded the result as:

1. Wall deflection increased with the increased compaction effort.
2. Residual lateral earth pressure increased near the top of the wall with increased compaction effort and decreased near the base of the wall. This decrease actually resulted from the relaxation of stresses due to the increased wall deflections.

Furthermore, Aggour and Brown used the same soil-wall geometry except that the last soil lift placed was compacted. The result was summarized as:

1. Wall deflection was increased.
2. The residual lateral earth pressure near the top of the wall was increased and a slight reduction of residual lateral pressures at deeper depth as a result of stress relaxation.

These results generally agree on a qualitative basis with field and scale-model observations based on the effects of compaction on structural deflections and residual lateral earth pressures.

Hua and Shen (1987) presented an analytical solution for an earth retaining structure that derives its stability from anchor plates placed in the granular backfill soil. Based on the parametric study, it was found that the most significant factor which could effects the lateral earth pressure and the amount of movement of the wall is the ratio of the area of an anchor plates to the area of the retaining wall. For a given state of stress, they postulated mathematical solution (between at rest and active) for lateral earth pressure distribution behind a retaining wall as follows:

$$P_c = \gamma Z \frac{A^2}{B} \mp \frac{1}{2}\gamma Z^2 \left[\frac{A(1+A^2)}{B^2}\right]\left(B - \frac{M}{2}A^2\right)\left[\varphi(1-B_j)\frac{1}{H}\right] \ldots\ldots\ldots\ldots\ldots\ldots (2.4)$$

Where, P_c= calculated lateral earth pressure at depth Z under a stress state B_j; H= height of the wall; ϕ= angle of internal friction of granular backfill; γ= unit weight of backfill; $A = \tan(45^0 - \psi/2); B = 1 + W/2(1 - A^2); M = \tan\theta/\tan\varphi$; θ = angle of wall friction; and ψ=angle representing the direction of resulting force on the wall.

Using this approach, it was possible to limit the lateral movement of the wall; however it had the following shortcomings:

1. This analysis was based on the limit equilibrium condition of the completed structure;
2. The construction sequence and the accompanying deformation of the system during construction were not considered in the solution;
3. Hence the analytical solution was acted like a conservative one, which may give larger lateral movement that a structure may be experienced in the field.

Duncan, William, Shen and Seed (1991) developed charts to estimate quickly the lateral earth pressures for highly overconsolidated sand. Theses charts were developed using the hysteretic theory proposed by Duncan and Seed (1986) with a computer program called EPCOMP2. This computer based program offered an advantage of being easy to use and provided very rapid results.

The charts proposed together with the adjacent factors were developed through the parametric studies using hysteretic computer analyses. They provided a simplified method of making accurate and also straightforward estimation of earth pressures due to compaction on nonyielding wall.

Field measurements of compaction induced earth pressure on a wall indicated that the horizontal earth pressure generated by the compaction of sand did not change appreciably

with time unless the wall moved toward or away from the backfill. Movement of a wall away from the backfill reduced the earth pressure below their after-compaction values while towards movement of the wall increased the earth pressure values compared to that of after-compaction. Comparisons of earth pressures calculated using these charts indicated that the values are sufficiently accurate for the practical purposes.

Clayton and Symons (1992) performed an analytical study on the pressure of compacted fill (both granular and stiff clay) behind a retaining wall. They reported that the classical earth pressure theories did not consider the construction process. They assumed that the corresponding increase in the horizontal pressure $\Delta\sigma_h$ imposed by the roller is $k_o\Delta\sigma_v$ for a rigid wall and $k_a\Delta\sigma_v$ for a yielding wall. Neglecting the self-weight of the fill; they expressed the maximum residual horizontal earth pressure as,

$$\sigma_{hrm} = \sqrt{(2p\gamma/\pi)} \quad \ldots(2.5)$$

Where, p = the roller load/unit width and should be doubled for vibrating roller.

γ = unit weight of soil.

From this approach, it is possible to predict the maximum residual horizontal earth pressure that is governed by the imposed loading and is independent of the strength properties of soil. Finally they concluded that compaction could increase the stresses acted on a retaining wall significantly above those predicted by the conventional earth pressure theories. Furthermore, the predictions of the earth pressure in granular soil using simple equation are in reasonable agreement with observations.

The shortcomings of their observation are:

1. The horizontal pressure and the critical height are overestimated as compared to the real values;

2. They assumed an infinitely distributed line load but in practice the roller has a finite dimension.

Using the same concept of Coulomb, Wang (2000) presented a formula for predicting the unit earth pressure acting against a retaining wall due to the thrust exerted by the sliding wedge of soil. A first order differential equation was set up by considering the equilibrium forces on element of wedge and proposed this theoretical formula as follows:

$$P_Y = \left[q - \frac{\gamma H}{aK-2}\right]\left[\frac{H-y}{H}\right]^{aK-1} + \left[\frac{\gamma H}{aK-2}\right]\left[\frac{H-y}{H}\right] \quad \ldots\ldots\ldots\ldots\ldots\ldots\ldots\ldots (2.6)$$

And $P_x = KP_Y$; here K= lateral earth pressure coefficient

$$a = \frac{\cos(\theta-\varphi-\delta)\tan\theta}{\sin(\theta-\varphi)\cos\delta} \quad \ldots\ldots\ldots\ldots\ldots\ldots\ldots\ldots\ldots\ldots\ldots\ldots\ldots\ldots\ldots\ldots (2.7)$$

The resultant earth pressure on the wall is:

$$P = \sqrt{(P_X^2 + T_1^2)} = \left[qH + \frac{1}{2}\gamma H^2\right]\left[\frac{\sin(\theta-\varphi)\cot\theta}{\cos(\theta-\varphi-\delta)}\right] \quad \ldots\ldots\ldots\ldots\ldots\ldots\ldots\ldots (2.8)$$

Here $T_1 = \int_0^H \tau_1 dy$

He also found that the height of resultant earth pressure where it was linearly distributed can be expressed as:

$$H_p = \frac{1}{3}H\left[\frac{3q+\gamma H}{2q+\gamma H}\right] \quad \ldots\ldots\ldots\ldots\ldots\ldots\ldots\ldots\ldots\ldots\ldots\ldots\ldots\ldots\ldots\ldots (2.9)$$

But for q = 0, $H_p = \frac{H}{3}$

2.3 Laboratory Studies

Terzaghi (1934) reported the results of a series of tests on a large earth pressure test apparatus using angular, medium, uniform sand as backfill. The sand was either damped in the loose state or compacted behind a modeled wall that could either rotate or move laterally. The average hydrostatic ratio (K_o) of the loosely damped sand corresponded well to the at-rest conditions but the pressures in the compacted sand were appreciably higher. The active condition occurred both for compacted and loosely damped sand when the rotation of the wall was allowed. However, in case of lateral translation without rotation, compacted sand mass only created the active state.

Davies and Stephens (1956) studied lateral earth pressures in a cubic container where the soils were compacted in a single lift by various means and to various degree of compaction. Due to the influence of scale, geometry and the uncertain nature of the deflection of the container, the result could not be rigorously assessed on a quantitative basis. However, they were able to conclude that these pressures increase appeared to be greatest towards the top of the container.

Sower et al. (1957) reported the results of series of laboratory tests specifically designed to measure the residual lateral earth pressures induced by static compaction on a cohesionless soil and also made a comparison between the sand and clay specimen. Owing to the geometry of the apparatus and the effects of adhesion and friction of the sides of the container, it was difficult to asses the results. It might be observed that residual pressures increased with the effective compactors weights. Thus, the cohesionless soils with less effective vertical confinement than the clay generally retained less residual lateral pressures because of absence of wall adhesion.

Rinkert (1959) performed half-scale tests on lateral earth pressures acting on a rigid wall using cohesionless soils. He reported that a significant amount of lateral stresses increased within the soil mass due to the application of a surface load to overconsolidate the soil and still remained after the removal of the overburden. The subsequent loading and unloading of the soil had little effect on the residual lateral earth pressures.

Brooker and Ireland (1965) performed an experimental investigation on the impact of soil stress history on the earth pressure at rest. They postulated that the stress history governed the values of K_o and an increase in the OCR reflected an increase in K_o. They also proposed that at higher values of OCR, the values of K_o appeared to reach the coefficient of passive earth pressure $K_p = (1+\sin\phi)/(1-\sin\phi)$

Schmidt (1966) further investigated the test results obtained by Brooker and Ireland. He proposed a simplified equation to correlate the coefficient of earth pressure at rest for normally consolidated soil (NC) [$K_{o(NC)}$] with the coefficient of earth pressure in rebound [$K_{o(R)}$], and the OCR.

$$K_{o(R)} = K_{o(NC)}(OCR)^b \quad (2.10)$$

Alpan (1967) analyzed the experimental data presented by Brooker and Ireland and presented an empirical formula similar to Schmidt's equation.

Hanna and Carr (1971) made an investigation to examine the loading behavior of plate anchors in normally consolidated and overconsolidated sand. They developed an apparatus with which desired stress state in the sand could be created. They also showed that the shape of the uplift load verses upward displacement diagram changed with OCR

and the peak uplift load increased with increase of the OCR. They concluded that the theoretical prediction of anchor load would only be possible when the stress strain system within the soil mass and also the stress history in the ground due to the anchor installation were known.

Al-Hossaini and Townsend (1975) examined specimens of loose and dense dry sands in the laboratory. The desired densities of the specimens were achieved by the vibrating each layer with a hand held hammer. They finally concluded that K_o increased with increasing OCR and also with the increasing applied compactive effort to the sand layers. They also suggested that the K_o values provide the good agreement with Jaky's equation.

Worth (1975) proposed the following relationship to calculate the coefficient of earth pressure at rest considering the OCR and Poisson's ratio μ.

$$K_{O(oc)} = K_{O(nc)} \times OCR - \left[\frac{\mu}{1-\mu}\right](OCR-1) \quad \ldots\ldots (2.11)$$

Only limitation of this formula is that it is valid for slightly overconsolidated soil where OCR $\leq$5 and Poisson's ratio ranging between 0.254 and 0.371.

Meyerhof (1976) proposed a semi empirical formula for approximate the estimation of K_o for overconsolidated soils and can be written as:

$$K_{o(OC)} = (1-\sin\phi)\sqrt{OCR} \quad \ldots\ldots (2.12)$$

Sherif and Mackey (1977) conducted an experimental investigation on the pressure acting on the retaining walls due to compaction. They postulated that 40 to 90% of the peak lateral earth pressure that was induced during compaction might remain as residual pressures. They also reported that previously compacted sands developed higher

increase in peak earth pressures when it was subjected to additional compaction and this caused an increase in K_o values.

Anderson and Hanna (1977) performed a series of laboratory tests on anchored retaining walls supporting cohesionless soil. They examined the behavior of wall supported by horizontal anchors as well as the effect of anchor inclination with increasing OCR. They found that the soil stress history had a very significant effect on the wall and retained sand behavior and finally they summarized their investigation as:

1. Increasing anchor inclination at higher OCR may cause higher horizontal earth pressure which may further cause greater wall movement;
2. Wall base reaction increases with increasing anchor inclination and therefore bearing capacity failure should be considered during design;
3. Increasing the anchors loads may control the movement of retaining wall.

Ranjan and Kaushal (1978) performed a small-scale laboratory test to investigate the load displacement characteristics of vertical anchor plates that buried in sand and experienced horizontal pull out. They used different sizes of the anchor plate at different embedded depth to investigate the factors affecting the anchorage capacity and also the displacement at failure. Finally, they concluded their obtained results as:

1. Anchorage capacity increases with the increasing plate size and embedment depth ratio. It is correspondingly less in medium sand, compared to that of dense sand and finally approaches to a constant value;
2. The displacement at failure increases with increasing the plate size and depth of embedment;
3. A shape factor of 1.2 was introduced for square anchors.

Clemence and Pepe (1984) conducted an experiment by installing soil stress cell into sand deposit to measure the lateral stress around the installation path of multihelix anchors before and after the installation process. They found that the values were considerably higher than that proposed by Jaky. They finally concluded that vibratory densification of soil induced lateral earth pressure that could lock into the soil and this, consequently, was reflected on the values of K_o.

Frydman and Shaham (1989) investigated the pullout capacity of slab anchor in homogeneous sand which depends on several factors including the type and density of the soil and depth, size, inclination and shape of the anchor slab. To calculate the pullout capacity of anchor, they proposed an expression for shape factor and inclination factor.

Hanna and Ghaly (1992) conducted experimental and theoretical studies on the effects of K_o and OCR on the uplift capacity of screw anchors on sand. Tests were conducted on prototype model. Predetermined relative densities were achieved by vibratory compaction of sand resulted an overconsolidated condition. Based on the stresses measured from experiments, the values of OCR was determined for all tested depths and sand types. They further proposed a semi-empirical relationship to relate the uplift capacities of screw anchor installed in overconsolidated sand to those installed in normally consolidated sand. They found a good agreement when the experimental results were compared with the results of a theory reported in the literature after incorporating the effect of OCR.

Filz and Duncan (1996) evaluated the theory proposed by Duncan and Seed (1986) by comparing the calculated and measured compaction-induced lateral earth

pressures. The measurements from three different stiff walls confirm the existence of compaction-induced lateral earth pressures.

They summarized their analysis in the graphical form stated below:

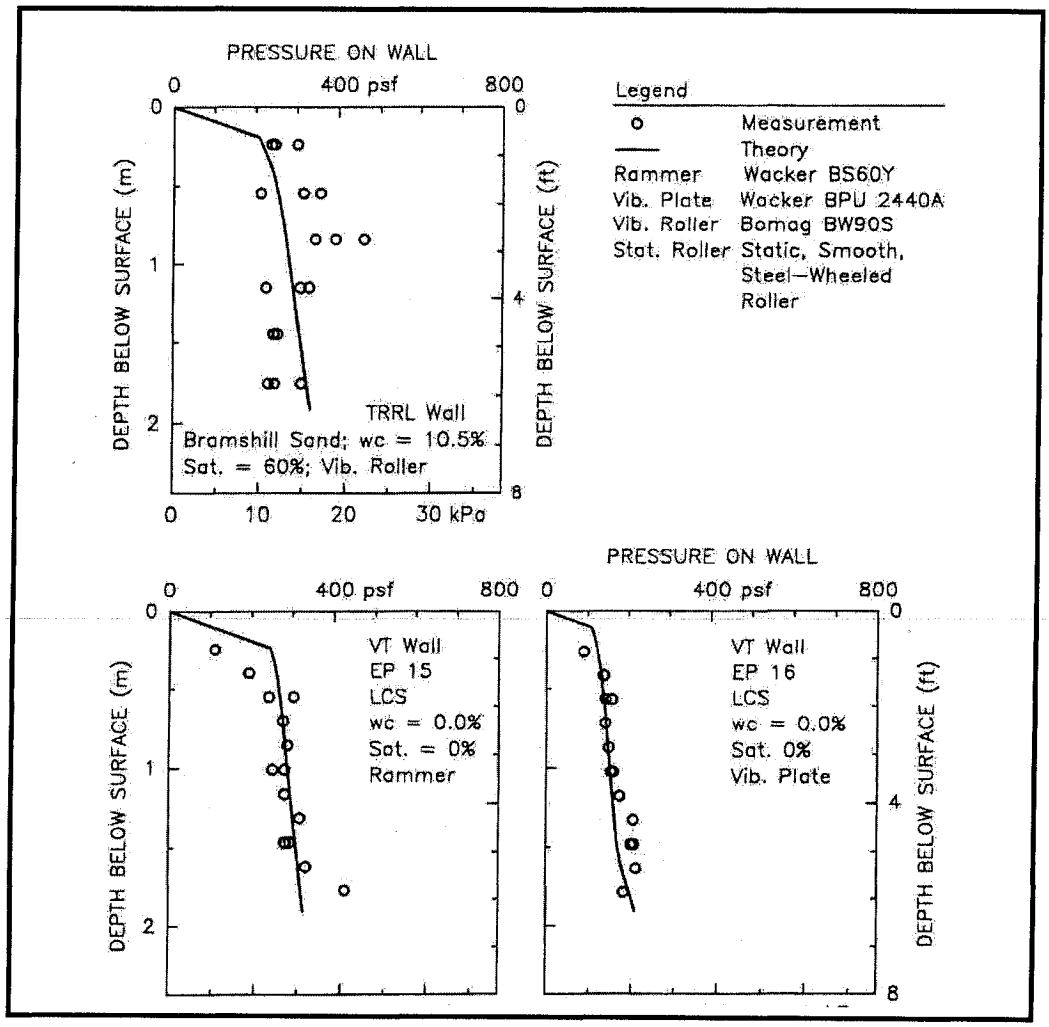

Figure 2.4 Lateral earth pressures for model wall tests with the sand backfills, Filz and Duncan (1996)

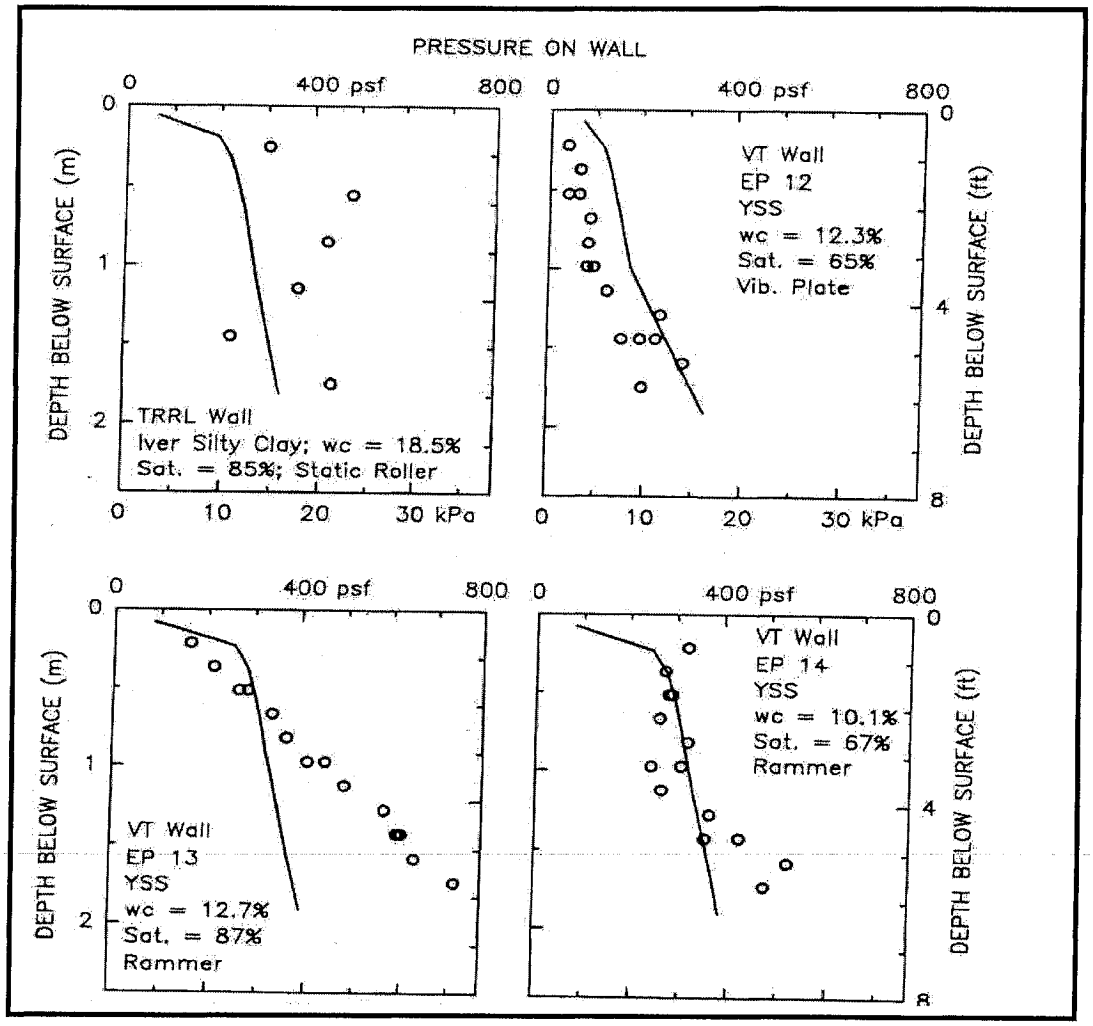

Figure 2.5 Lateral earth pressure for the model wall tests with moisture-sensitive silty and clayey backfills, Filz and Duncan (1996)

Good agreement was found between the Duncan and Seed (1986) compaction-induced lateral earth pressure theory and the measured values obtained from three tests in which sand was used as backfill. Therefore, the theoretical predictions of compaction-induced lateral earth pressure were more difficult for the silty and clayey soils as significant pore water pressure was developed during placement and compaction.

Hanna and Saad (2001) presented the results of an experimental investigation on a prototype model. The effect of compaction duration on the mechanical properties and the induced stress levels in the sand mass was examined. They further presented their results to develop some awareness about the validity of using the results of model testing as a guide in developing design theories. Furthermore, they attempted to measure and incorporate the governing parameters in the in-situ stress level and in the design theories. The purpose of this study was to evaluate the effectiveness of using the results of the laboratory testing in developing design theories.

Based on the results of their study, the following conclusions were drawn:

1. Sand placing technique has a significant influence on the measured mechanical properties and *OCR* values that increasing with depth;
2. Energy input to the sand layer during compaction has a dominant influence on the in-situ stress level; higher energy input causes higher in situ stresses and maximum energy conservation remains at the bottom layer;
3. Higher numbers of layers increase the unit weight and the angle of shearing resistance in the lower layers of backfill.

There might be some limitations like the scale effect of the test model, the difficulties in duplicating the boundary conditions of the prototype model and the development of a sand placing technique to simulate the particle arrangement and the in situ stress levels.

Massarsch and Fellenius (2002) reported the variation of the earth pressure in normally consolidated and overconsolidated soil. The effect of soil compaction on the horizontal effective stress was also discussed based on cone penetration test (CPT) data.

The results indicated a significant increase in cone stress and sleeve friction and a decrease in compressibility due to compaction.

Finally they concluded their analysis as:

1. Though the cone stress was influenced by the vertical and horizontal effective stress, it should be adjusted for the mean stress, rather than the effective overburden;
2. Soil compaction increased not only the soil density but also horizontal effective stress; a substantial increase in the overconsolidation ratio was also resulted by this compaction;
3. A case study results showed the sleeve friction increased proportionally and the friction ratio was unchanged.

Hanna and Khoury (2005) performed laboratory tests to investigate the passive earth pressure acting on a wall. The wall was retaining the overconsolidated homogeneous sand backfill and overconsolidated backfill overlying natural deposit. Different overconsolidation was achieved by compacting the soil mechanically for different period of time and found a good agreement with other experimental values. Finally they provided design charts and formulae for practical use as follows:

For smooth walls where $\delta = 0$ and homogeneous sand backfill,

$$K_{p(oc)} = b\sqrt{OCR}K_{p(nc)} \quad \ldots\ldots\ldots\ldots\ldots\ldots\ldots\ldots\ldots\ldots\ldots\ldots\ldots \quad (2.13)$$

b = constant given in a chart.

For rough walls ($1/2\phi < \delta < 2/3\phi$),

$$K_{p(oc)} = K_{p(nc)}\left\{1.5 - \left(\frac{\delta - 25}{100}\right)\right\}(OCR)^{\sin\delta} \quad \ldots\ldots\ldots\ldots\ldots\ldots\ldots\ldots \quad (2.14)$$

For non homogeneous sand layer,

$$K_p\left(\frac{backfill}{deposit}\right) = \left[\frac{K_p(backfill) + K_p(deposit)}{2}\right] \quad \ldots\ldots\ldots\ldots\ldots\ldots\ldots \quad (2.15)$$

Finally they concluded that:

1. Compaction induced additional stress in the backfill causes the material overconsolidated and accordingly increases the OCR as well as passive earth pressure;
2. OCR and the soil condition below the founding level affect significantly the coefficient of passive earth pressure;
3. When strong overconsolidated sand backfill overlying a weak deposit, the failure mechanism extends to the weak layer; it causes a significant reduction in the passive earth pressure acting on the retaining wall;
4. For the case of weak layer overlying strong layer, the failure mechanism is mobilized in the backfill material and strong deposit becomes undisturbed; so the wall experiences the passive earth pressure that occurs in the homogeneous soil system.

2.4 Summary and Discussion

A large number of laboratory and full-scale field studies on the lateral earth pressure and deformation of the wall have been performed during last 50 years. Nevertheless, most of the data available based on the compaction induced earth pressure measurements are of

limited values even with recent advanced technique to measure the in situ earth pressures. It remains difficult to obtain the reliable data with high accuracy even under ideal conditions.

Based on the available laboratory and field data, the following observation can be made regarding the compaction induced lateral earth pressures:

1. The compaction of soil, which is a process of load application and load removal, can significantly increase the residual lateral earth pressure within the soil mass. This residual pressure is sometimes much higher than the at rest values and may approach the passive earth pressure magnitude. At intermediate depth, the residual pressure increases rapidly while its increments are less rapid or fairly constant with depth and the earth pressure appears to be at-rest values;
2. Compaction of soil having higher OCR against a deflecting structure significantly increases the structural deflection. This deflection generally increases near the surface where the residual pressure is higher than at rest values and gradually decreases with depth;
3. The depth to which compaction increases, the lateral earth pressure appears to be a function of the dimensions and the vertical thrust of the compaction roller;
4. At depth where available pressure is sufficient and the possible earth pressure does not limit residual earth pressure, a high percentage of compaction induced peak lateral earth pressure may remain as residual pressure. However, additional compaction loading can result in much smaller increase in the peak lateral earth pressure at this stage.

5. The in-situ stress level also depends on the sand placing technique and also the energy input within the soil mass during compaction. Higher energy input causes higher unit weight with increasing depth and also increases in angle of shearing resistance with depth;
6. Compacted backfill locks the additional stress within the soil mass and thus increase OCR and passive earth pressure;
7. In layered soil system, strong backfill layer has significant effect on passive earth pressure acting on retaining structure;
8. In case of earth anchors, size and depth of embedment plays an important role to derive the anchorage capacity and its displacement.

From the above discussion, it is quite clear that the researchers, in most cases, assumed that the soil was at-rest condition before and after compaction using mechanical efforts or applying surcharges. But in reality, the behavior and the lateral earth pressure of the compacted soil mass could be different. Most of the time, it could exceed the at-rest values. Furthermore there was no attempt to measure the lateral earth pressure behind an earth anchor plate.

2.5 Research Objective

The objective of this thesis is to investigate the stress condition of the soil behind a rigid, non-yielding retaining wall as well as in front of an embedded earth anchor plate connected to a rigid non yielding retaining wall. By compacting the backfill soil at different limits, the OCR of the backfill material will be changed and the passive earth pressure will be analyzed under different soil condition (normally or overconsolidated).

Finally, a design procedure will be provided for the anchor plate through proposed charts and design formulae. A comparison will also be made with the data available. In order to reach the goal, following steps will be followed in this research program:

1. To prepare the literature review of the subject;
2. To develop a numerical model of a wall retaining homogeneous or overconsolidated soil overlying natural deposit, to examine the effect of overconsolidation on the coefficient of passive earth pressure on these walls;
3. To develop a numerical model of a horizontal anchor in homogeneous soil, to evaluate the coefficient of residual lateral earth pressure in front of an embedded anchor plate at different OCR, overburden and soil condition (loose, medium and dense) using Mohr-Coulomb Model;
4. To validate these models with the available experimental data;
5. To develop design theories and empirical formulae to predict the passive earth pressure behind walls and anchor plates for a wide range of overconsolidation ratio, embedment ratio and plate rotation.

CHAPTER 3

NUMERICAL MODELING

3.1 General

In recent years, finite element method is considered as the most powerful and widely accepted technique to solve the problems in the field of geotechnical engineering. In this present study, numerical models were developed using the 2-D finite element technique. One model considered the vertical nonyielding rigid wall in a homogeneous sand backfill while in another model; the same wall retained overconsolidated backfill overlying natural deposit. The third model consisted of a vertical anchor plate which was embedded in homogeneous backfill and was screwed with a rigid vertical wall. Several trials with different constitutive laws were performed and it was decided to use the Mohr-Coulomb model in the present numerical analysis. After validation of the numerical models, the models were then used to generate data for a wide range of the governing parameters.

3.2 Numerical Models

Finite Element Modeling is a method where a continuum is divided into a finite number of elements and each element is further consisted with finite number of nodes. Higher number of elements with higher number of nodes comprises higher accuracy. In these numerical models, a plane-strain model with 4^{th} order 15-node triangular elements was considered to provide finest distribution of stress strain and thus produce more accurate results.

3.3 Geometry and Boundary Condition

The geometry of the first model was described as a homogeneous single layer backfill consisted of a vertical and rigid retaining wall. The retaining wall in this numerical model was considered as plate element with material properties of concrete. The soil system was defined as sand with different values of stiffness, OCR and constant Poisson's ratio. Figure 3.1 describe the geometry of the first model consisted of vertical wall in homogeneous soil system.

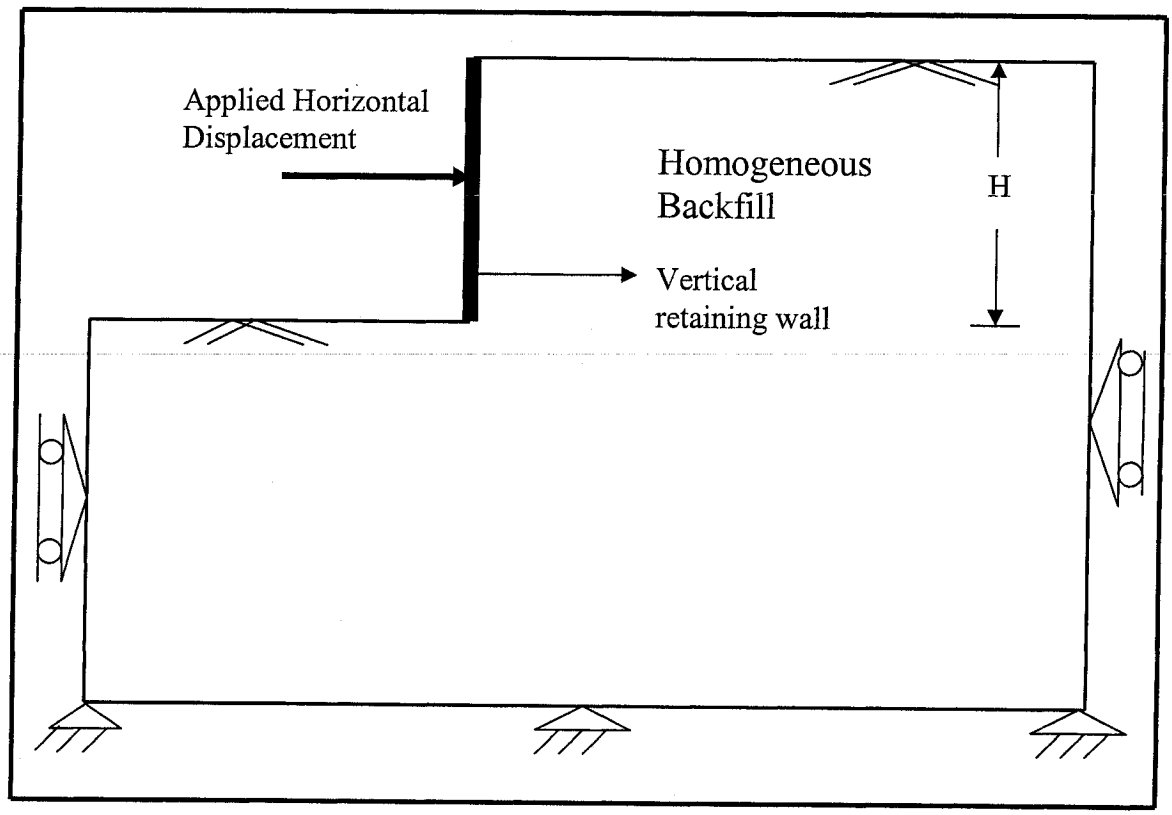

Figure 3.1 Geometry of the numerical model with vertical wall in homogeneous backfill

The second model considered a vertical anchor plate screwed with a rigid nonyielding retaining wall. The backfill material in which the anchor was embedded was a homogeneous sand layer with different OCR. Plate element was used to construct the retaining wall, anchor plate and anchor rod with different material properties. The concrete material was assigned to model the plate element of retaining wall where as properties of steel were used to develop the anchor rod and anchor plate. Backfill materials were the same as considered in the first numerical model. Figure 3.2 shows the numerical model with vertical anchor plate embedded in a homogeneous soil system.

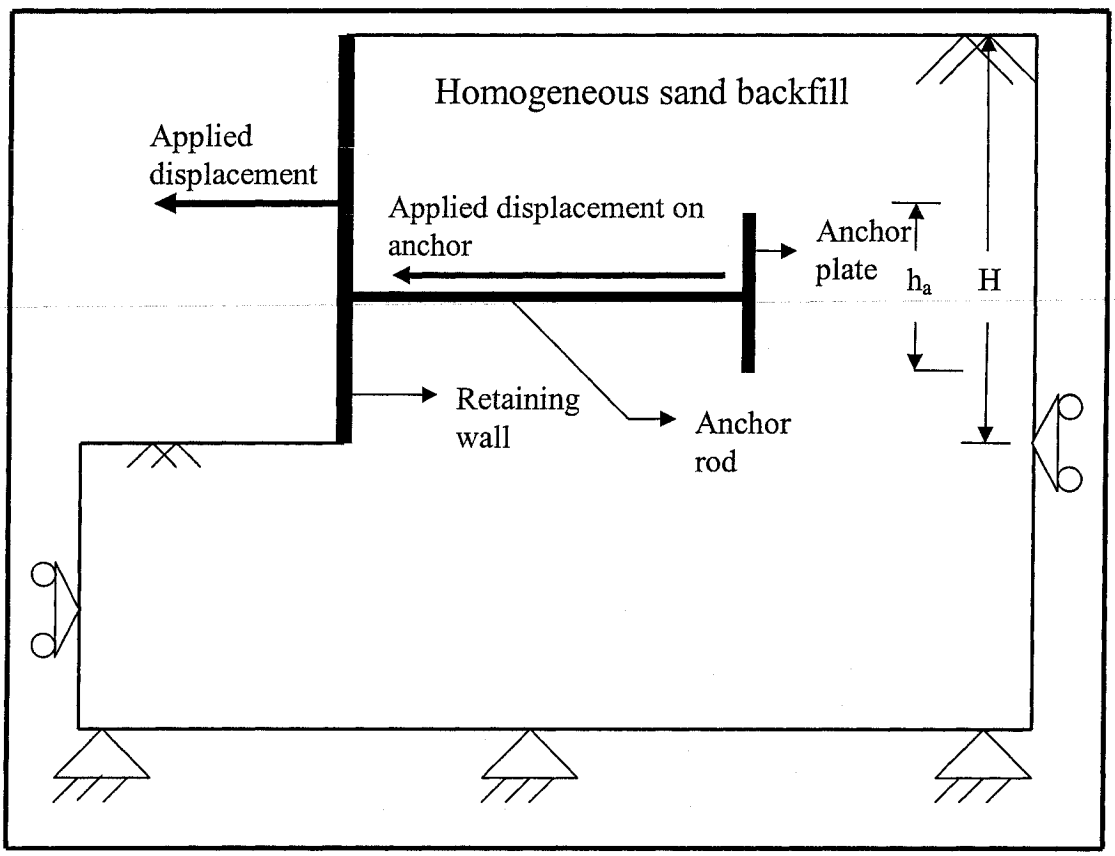

Figure 3.2 Geometry of the numerical model - vertical anchor plate embedded into homogeneous backfill

The third numerical model was developed with a vertical, rigid wall which retained the overconsolidated backfill overlying natural deposit. The backfill materials were slightly compacted with OCR varied from 2 to 4, while the underlying soil below the toe of the vertical wall was kept undisturbed. The material properties of the wall and the backfill soil layer were the same as considered in the first model. Figure 3.3 illustrates the geometry of the numerical model with a retaining wall in layered soil.

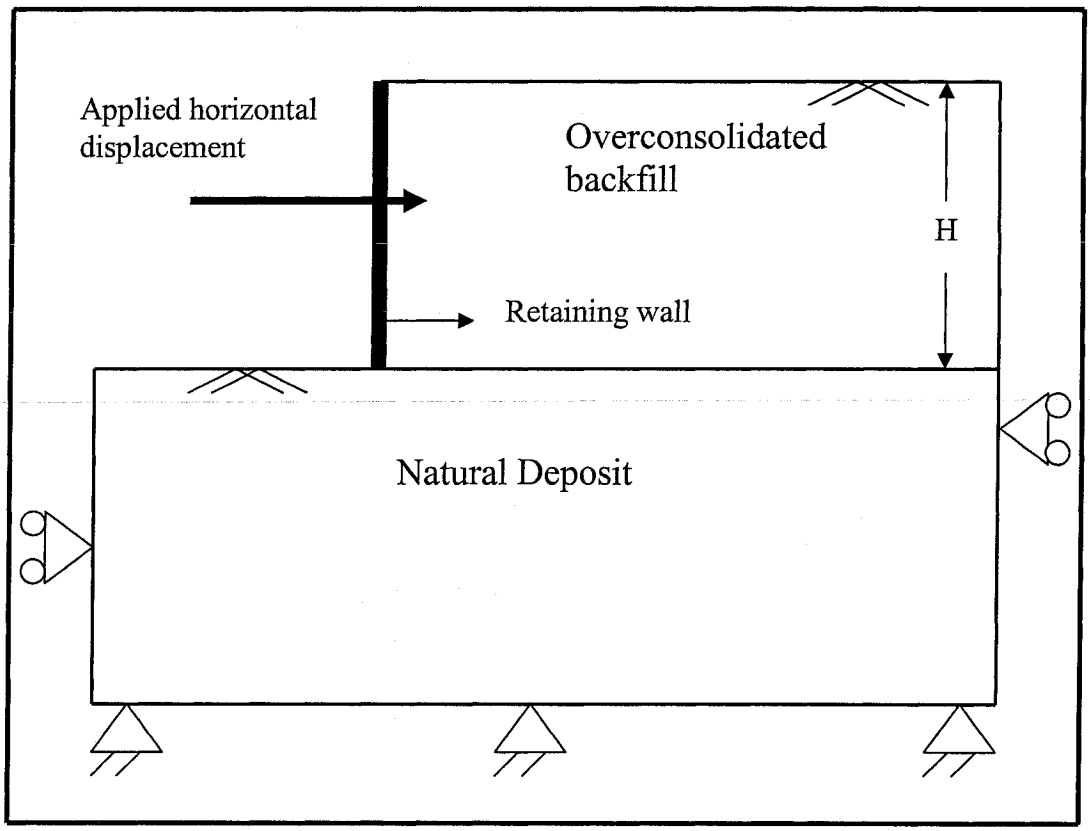

Figure 3.3 Geometry of the numerical model with wall retains overconsolidated backfill overlying natural deposit

The boundary of these numerical models was established by several trials with different dimensions of soil body. At first, a smaller boundary, same as the experimental investigation (1.080 m × 0.197 m × 0.477 m) performed by Hanna and Khoury (2005), was chosen to estimate the passive earth pressure. The measured earth pressure was gradually decreasing with increasing dimensions of the boundary. Finally, the dimension of the soil body was set with a depth of 30m which was greater than 1.5H (height of the retaining wall) and the length was 50m which was greater than the length of anchor rod. Length of anchor rod was calculated using the following formula:

$$L_a \geq H \tan\left(45^0 - \frac{\varphi}{2}\right) + D' \tan\left(45^0 + \frac{\varphi}{2}\right) \ldots\ldots\ldots\ldots\ldots\ldots\ldots\ldots\ldots \quad (3.1)$$

Where, H = height of the retaining wall

D' = depth of the bottom of anchor plate from top of the soil layer.

The width of the boundary was always 1m as the models were developed considering the plain strain problem. The geometry was selected in such a way to eliminate both horizontal and vertical stress confinement within the soil boundary. It was found that the calculated earth pressure were almost constant when the dimensions were slightly below or above this selected boundary. Hence, the dimension of the soil body to develop the numerical models was selected as 50 m ×1 m × 30 m to eliminate the confinement of the stress level.

The outer boundaries of the soil model were supported by standard fixities. Fixed support was considered at the bottom of the mesh and hinged supports were on both horizontal directions as shown in figure 3.1, 3.2 and 3.3 above. These outer boundaries ensured that an increase in stress due to wall movement within the boundary was absorbed without rebounding. Both loading and sequence of construction were

multistage. Water level was considered at infinite depth and hence the soil was fully unsaturated with PWP = 0.

3.4 Mohr-Coulomb Model

In this study, an elastoplastic Mohr-Coulomb failure criterion was considered as the most effective constitutive law to estimate the lateral earth pressure. Mohr (1900) proposed a theory for rupture in material according to which the failure occurs with a critical combination of normal and shear stresses within a material. He expressed the functional relationship between the shear and normal stresses on a failure plane as:

$$\tau = f(\sigma) \quad \ldots (3.2)$$

This failure envelop is a curved surface which in most case is sufficient to approximate the shear strength on a failure plane as linear function of the normal stresses and known as Mohr-Coulomb equation. The governing equation of Mohr-Coulomb model represents (figure 3.4) the first order approximation and can be stated as follows:

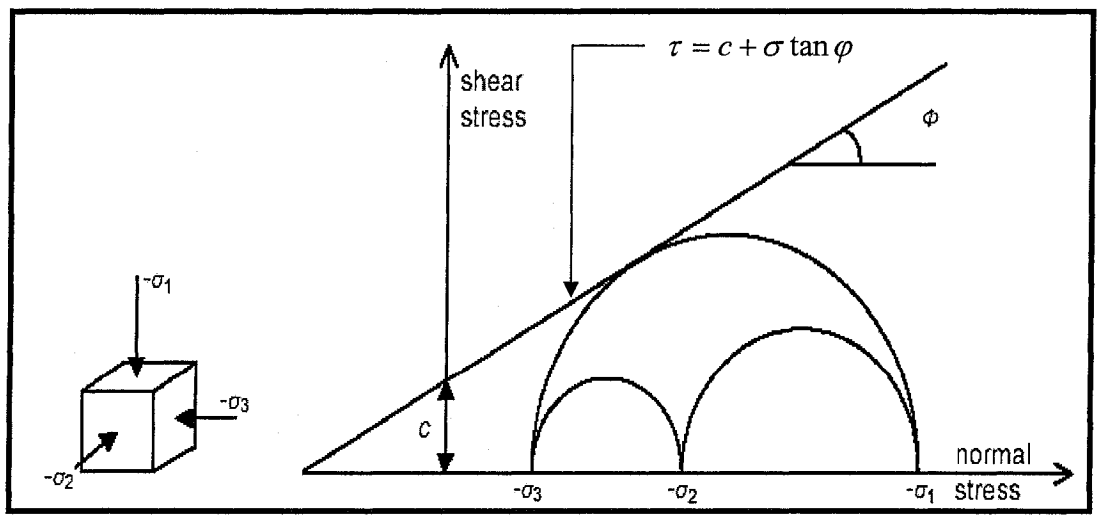

Figure 3.4 Mohr-Coulomb failure envelope

$$\tau = \sigma \tan \varphi + c \ldots \ldots \ldots \ldots \ldots \ldots \ldots \ldots \ldots \ldots \ldots \ldots \ldots \ldots \ldots \ldots \ldots \ldots \ldots \ldots \ldots \ldots (3.3)$$

Here, τ = shear strength of soil

σ = normal stress

c = cohesion

ϕ = angle of internal friction of soil body.

3.4.1 Basic Parameters of Mohr-Coulomb Model

Mohr-Coulomb model requires five basic input parameters such as:

E = modulus of Elasticity of soil	[KN/m^2]
ϕ = angle of internal friction within soil mass	[^{0}]
μ = Poisson's ratio of soil	[-]
ψ = angle of dilatancy	[^{0}]
c= cohesion	[KN/m^2]

In present study, ϕ was considered in the range of 30^0 to 45^0 with OCR varied from 1 to 4. The angle of dilatancy (ψ) was normally considered as zero for loose sand ($\phi \leq 30^0$). But for the heavily overconsolidated sand or medium to dense sand, the general formula for dilatancy is $\psi = (\phi - 30^0)$. The Poisson's ratio for granular soil generally varies from 0.28 to 0.3. Thus, a constant value of μ between these ranges was considered. Young's modulus, E, varies a wide range under different stress conditions. For sand, normally cohesion c = 0 but according to the PLAXIS manual, c must >0.2. A value of 0.5 was assigned in the present numerical models to avoid complication.

3.5 Soil Elements

15-node triangular elements were used to model the soil material and other volume of clusters. It presented a fourth order interpolation for the displacements and the numerical integration of stress points (Gauss points). Input data set for soil element is presented in table 3.1.

Table 3.1 Properties of soil and interface elements

Parameter		Units	Assigned values
Material type	Sand	-	
Material model	Mohr-Coulomb	-	
Type of material behavior	Drained	-	
Soil unit weight (γ_{dry})	$\phi = 30^0$	kN/m^3	16.0
	$\phi = 35^0$		18.5
	$\phi = 40^0$		19.0
	$\phi = 45^0$		19.5
Soil unit weight (γ_{sat})	$\phi = 30^0$	kN/m^3	19.5
	$\phi = 35^0$		20.0
	$\phi = 40^0$		21.0
	$\phi = 45^0$		22.0
Young's modulus (E)	Variable	kN/m^2	Proposed Chart
Poisson's ratio (μ)	constant	-	0.3
Angle of shearing resistance (ϕ)	Variable	Degree	30
			35
			40
			45
Angle of dilatancy, ψ	Variable	Degree	0 for ϕ=30
			5 for ϕ=35
			10 for ϕ=40
			15 for ϕ=45

In present investigation, the OCR was one of the most important variable parameter, which significantly affected the coefficient of lateral earth pressure. However, the major limitation of Mohr-Coulomb model used in finite element simulation was that the value of OCR was introduced as a function of K_o, coefficient of earth pressure at-rest, while E was one of the basic input parameters in Mohr-Coulomb model (section 3.4.1). The modulus of elasticity E, function of horizontal lateral earth pressure (σ_3), is a stiffness parameter of the soil where as OCR is the strength parameter which only depends on the vertical stress (σ_1). Correlation between these two parameters, which was not available in the existing theories, was obvious due to analyze the effect of OCR on the lateral earth pressure. To overcome this shortcoming of the Mohr-Coulomb model, the following steps were considered to obtain the correlation and a design chart was presented using the available theories.

Step 1: The coefficients of earth pressure at rest for different OCR were calculated using the following formula proposed by Meyerhof (1976).

$$K_{o(oc)} = (1 - \sin\varphi)OCR^{0.5} \quad \ldots\ldots (3.4)$$

Here OCR = over consolidation ratio (ranges from 1 to 4)

ϕ = angle of internal friction (ranges from 30^0 to 45^0)

Table 3.2 shows the values of coefficient of earth pressure at rest, K_o, for a wide range of OCR varies from 1 to 4. The values of K_o used in Mohr-Coulomb model describe the initial stress condition within the soil mass, which is further discussed in section 3.9.

Table 3.2 Values of $K_{o(OC)}$ at different OCR (using equation 3.4)

ϕ (degree)	γ_s (kN/m^3)	$K_{0(NC)=OCR(1)}$	$K_{o(OCRR=2)}$	$K_{o(OCR=3)}$	$K_{o(OCR=4)}$
30	16.5	0.5	0.707	0.866	1.00
35	18.5	0.426	0.603	0.739	0.853
40	19.0	0.357	0.505	0.619	0.714
45	19.5	0.293	0.414	0.507	0.586

Step 2: The vertical and horizontal earth pressure on a soil element were calculated using the following formula:

$$\sigma_1 = \gamma_s h \quad \ldots \quad (3.5)$$

Here $\sigma_1 = \dfrac{\sigma_{11} + \sigma_{21}}{2}$

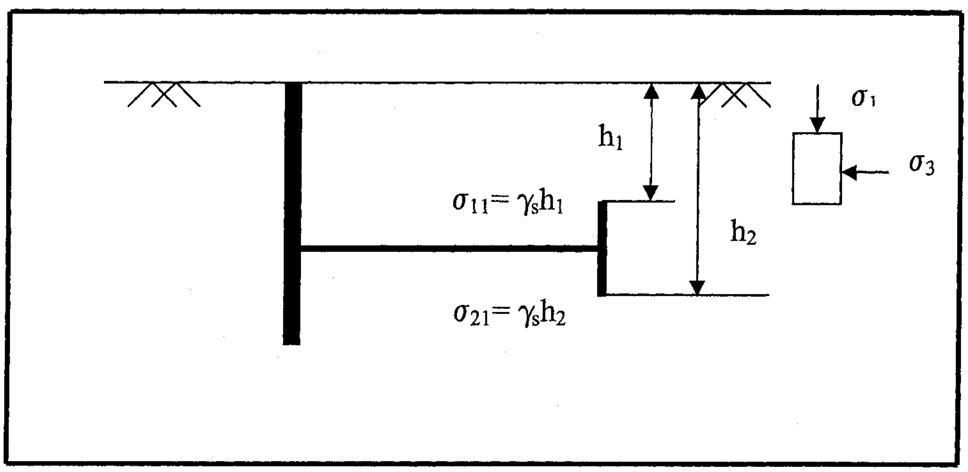

Figure 3.5 Calculation of vertical effective stress on anchor plate at any arbitrary embedded depth

$$\sigma_3 = K_{o(OC)}\sigma_1 \quad \ldots (3.6)$$

Table 3.3 shows the calculated value of σ_3 for different ϕ and OCR considering any arbitrary height, $h_1 = 3$ m and $h_2 = 5$ m

Table 3.3 Variation of horizontal earth pressure with ϕ & OCR (using equation 3.6)

ϕ (degree)	$\sigma_{3\,(OCR=1)}$ (kN/m^2)	$\sigma_{3\,(OCR=2)}$ (kN/m^2)	$\sigma_{3\,(OCR=3)}$ (kN/m^2)	$\sigma_{3\,(OCR=4)}$ (kN/m^2)
30	33	46.67	57.16	67
35	31.56	44.63	54.66	63.11
40	27.15	38.39	47.02	54.3
45	22.85	32.31	39.57	45.69

Step 3: Young's modulus E, adopted from Janbu (1963) and reconfirmed by Duncan et al. (1980) was expressed by a relationship as:

$$E = KP_a\left(\frac{\sigma_3}{P_a}\right)^n \quad \ldots (3.7)$$

Where, K= dimensionless modulus number (range from 300 to 2000)

P_a= atmospheric pressure (101 kN/m^2)

n = exponent (range from 0.3 to 0.6)

The values of K and n were summarized by Wong and Duncan (1974) for different type of soil based on c and ϕ values.

Using the relation presented in equation 3.7 and the proposed values of K and n, E was calculated at different ϕ and OCR and presented in table 3.4.

Table 3.4 Values of E at different $K_{o(OC)}$ (using equation 3.7)

ϕ (degree)	K	n	Pa (kN/m^2)	$E_{(OCR=1)}$ (kN/m^2)	$E_{(OCR=2)}$ (kN/m^2)	$E_{(OCR=3)}$ (kN/m^2)	$E_{(OCR=4)}$ (kN/m^2)
30	722	0.62	101	36446.68	45183.23	51234.86	56014
35	1148	0.595	101	58028.38	71317.62	80460.74	87650.27
40	1574	0.567	101	75426.03	91820.25	10301.93	111777.85
45	2000	0.54	101	90525.71	109156.11	121785.25	131621.90

Step 4: Finally the following non-dimensional design chart presented in figure 3.6 was presented in present study to calculate the value of Young's modulus E at different OCR.

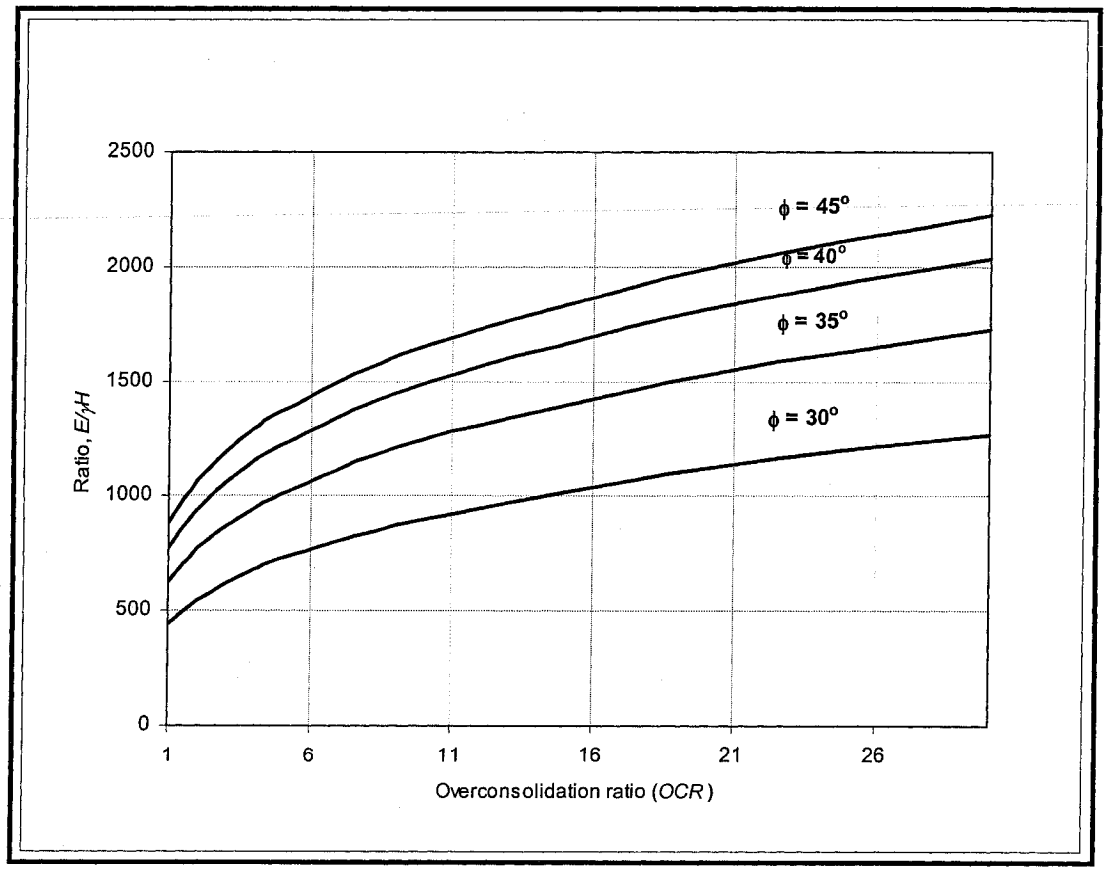

Figure 3.6 Design chart for Young's modulus, E and OCR using existing theories

3.6 Plate Elements

Plate elements were used to develop the numerical model of vertical wall, anchor rod and anchor plate. Elastic concrete material was used to simulate the retaining wall while anchor rod and anchor plate were considered as steel material. Tables 3.5 and 3.6 show the material properties of retaining wall, anchor rod and plate. Weight of the plate elements were calculated using the following formula:

$$W_{plate(orrod)} = (\gamma_{steel} - \gamma_{soil}) \times t_{plate(oranchorrod)} \quad \ldots (3.8)$$

$$W_{wall} = (\gamma_{concrete} - \gamma_{soil}) \times t_{wall} \quad \ldots (3.9)$$

Where, γ_{steel} = unit weight of steel

$\gamma_{concrete}$ = unit weight of concrete

γ_{soil} = unit weight of soil

$t_{plate(rod/anchor\ plate)}$ = thickness of anchor rod or anchor plate

t_{wall} = thickness of retaining wall

Flexural rigidity EI and axial stiffness EA were the two basic input parameters to model the plate elements from which equivalent plate thickness d_{eq} was calculated using the following equation:

$$d_{eq} = \sqrt{12\frac{EI}{EA}} \quad \ldots (3.10)$$

Table 3.5 Properties of Plate Element (retaining wall)

Parameter		Units	Assigned values
Material type	Concrete plate		
Type of behavior	Linear Elastic		
Material unit weight ($\gamma_{concrete}$)	Constant	kN/m^3	23
Young's modulus (E_c)	Constant	kN/m^2	1.10E+07
Axial stiffness, (EA)	Constant	kN/m	5.5E+06
Flexural rigidity, (EI)	Constant	$kN\text{-}m^2/m$	1.15E+05
Equivalent thickness, d_{eq}	Constant	m	0.5
Weight, W	$\phi = 30^0$	kN/m/m	3.25
	$\phi = 35^0$		2.25
	$\phi = 40^0$		2.00
	$\phi = 45^0$		1.75

Table 3.6 Properties of Plate Element (anchor rod and anchor plate)

Parameter		Units	Assigned values (anchor plate)	Assigned values (anchor rod)
Material type	Steel plate			
Type of behavior	Linear elastic			
Material unit weight (γ_{steel})	Constant	kN/m^3	76.87	76.87
Young's modulus (E_s)	Constant	kN/m^2	2.0E+11	2.0E+11
Axial stiffness, (EA)	Constant	kN/m	8.0E+10	3.2E+10
Flexural rigidity, (EI)	Constant	kN m^2/m	1.07E+09	4.27E+08
Equivalent thickness, d_{eq}	Constant	m	0.4	0.4
Anchor rod length	$\phi = 30^0$	m	-	13
	$\phi = 35^0$			14
	$\phi = 40^0$			14
	$\phi = 45^0$			15
Weight, W	$\phi = 30^0$	kN/m/m	24.15	24.15
	$\phi = 35^0$		23.35	23.35
	$\phi = 40^0$		23.15	23.15
	$\phi = 45^0$		22.95	22.95

3.7 Interface Elements

In this present study, the soil element consisted of 15 nodal points and hence the interface element was consisted of 10-nodes with 5 stress points. Figure 3.7 shows connection between the soil and the interface elements which were assumed to behave elastically to simulate the stress points between the soil and the plate elements. The roughness of the interface element varies from smooth to fully rough ($0 \leq \delta/\phi \leq 1$) and the roughness level was taken by choosing a suitable value for the strength reduction factor (R_{inter}).

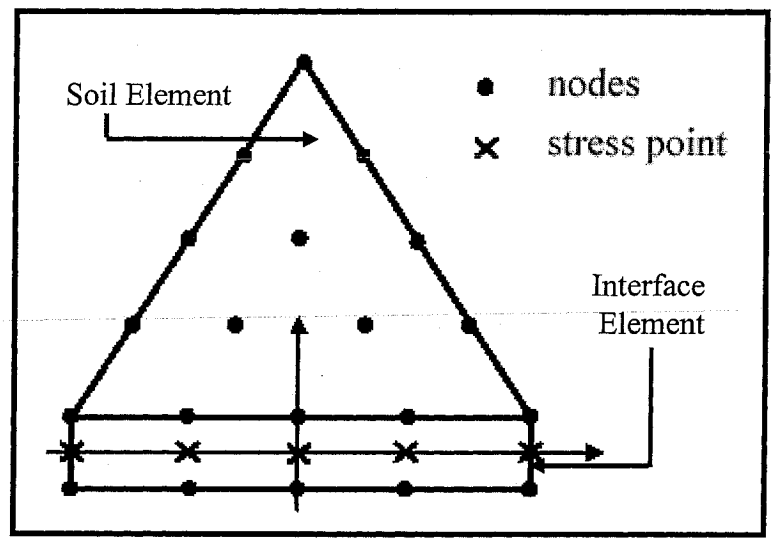

Figure 3.7 Distribution of node and stress points within the interface element and their connection to soil elements in finite element model

The interface properties were calculated from the soil properties in associated with data set and the strength reduction factor by applying the following rules:

$$\tan\varphi_i = R_{inter} \tan\varphi_{soil} \leq \tan\varphi_{soil} \quad \ldots\ldots(3.11)$$

$$\psi_i = 0 \text{ for } R_{inter}<1, \text{ otherwise } \psi_i = \psi_{soil}$$

Where, φ_i and φ_{soil} = frictional angle of interface and soil respectively

ψ_i = dilatancy angle of the interface

ψ_{soil} = dilatancy angle of the soil

Values of the strength reduction factors used in present study are presented in table 3.7 for soil and plate materials.

Table 3.7 Different values of strength reduction factor for different interface elements

Interface	Strength reduction factor, (R_{inter})
Soil/ Concrete retaining wall	0.67
Soil/Anchor rod	0.2
Soil/Anchor plate	0.33

A 'virtual thickness' value was assigned to each interface finite element model which was an imaginary dimension calculated from the virtual thickness factor multiplying with element size. The element size was determined from the global coarseness set in the 2-D mesh generation. Normally the virtual thickness factor is taken as 0.1 by default.

3.8 Mesh Generation

The average element size l_e was a required parameter to generate the mesh, which could be calculated using the outer geometry dimensions (x_{min}, x_{max}, y_{min}, y_{max}). The setting of the global coarseness was defined in the mesh as:

$$l_e = \sqrt{\frac{(x_{max} - x_{min})(y_{max} - y_{min})}{n_c}} \quad \ldots\ldots\ldots\ldots\ldots\ldots\ldots\ldots\ldots\ldots \quad (3.12)$$

Here n_c = global coarseness number.

Global coarseness was divided in five different levels presented in table 3.8. The selection of mesh global coarseness accomplished an acceptable degree of accuracy and computing time. Number of elements for various types of global coarseness is also presented in table 3.8.

Table 3.8 Number of elements for global coarseness in finite element model

Global Coarseness	n_e	No of elements
Very course	25	50
Course	50	100
Medium	100	250
Fine	200	500
Very fine	400	1000

In this investigation, the global coarseness was taken as medium with a more refined line at anchor plate-soil interface element and wall-soil interface element. Figure 3.8 (a) and (b) show a typical mesh generation and deformed mesh in model 2 before and after the horizontal displacement was applied to the wall accordingly.

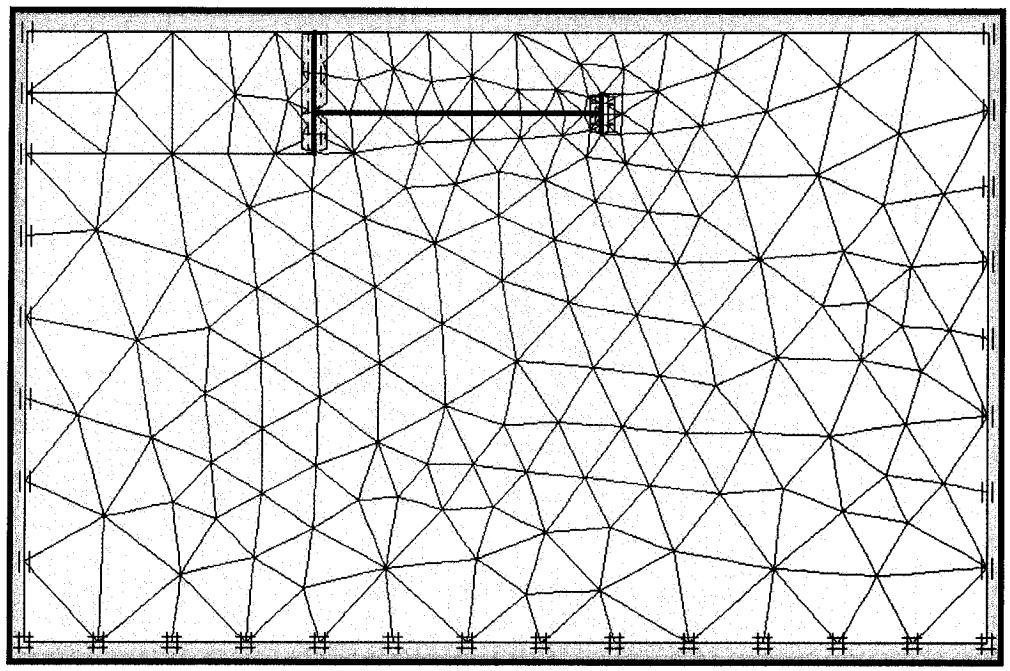

Figure 3.8 (a) Mesh generation (model 2) before horizontal displacement is applied

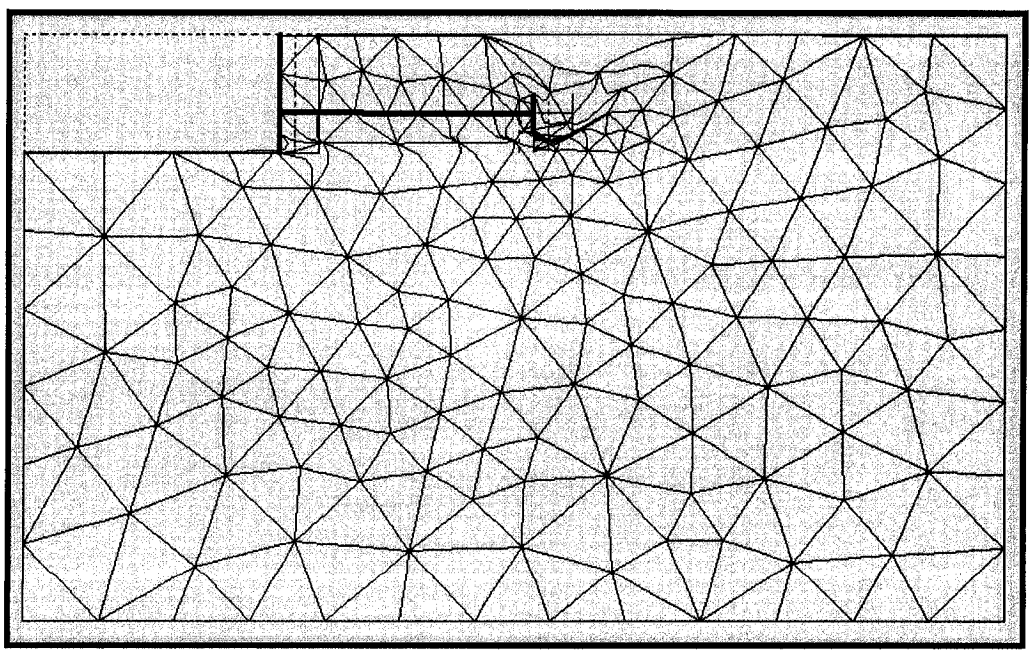

Figure 3.8 (b) Deformed mesh (model 2) after horizontal displacement is applied

3.9 Initial Stress Condition

Initial stress generation was the first step to obtain the model output. In present study, the numerical model calculated the initial stress in the soil mass using the following formula:

$$\sigma_{h,o} = K_0 \sigma_{v,o} \quad \ldots \ldots \ldots \ldots \ldots \ldots \ldots \ldots \ldots \ldots \ldots \ldots \ldots \ldots \ldots \quad (3.13)$$

The finite element model generated the initial stresses either by specifying K_0 or by using gravity loading. In present investigation, initial stresses were generated in Mohr-Coulomb model by assigning the value of K_0. The procedure to calculate K_0 was illustrated in section 3.5 and its variation with OCR was presented in table 3.2.

After the initial stresses were generated, the output program was started. Figure 3.9 illustrates the initial stress condition when the entire soil body was at rest and no displacement was experienced by the earth structures.

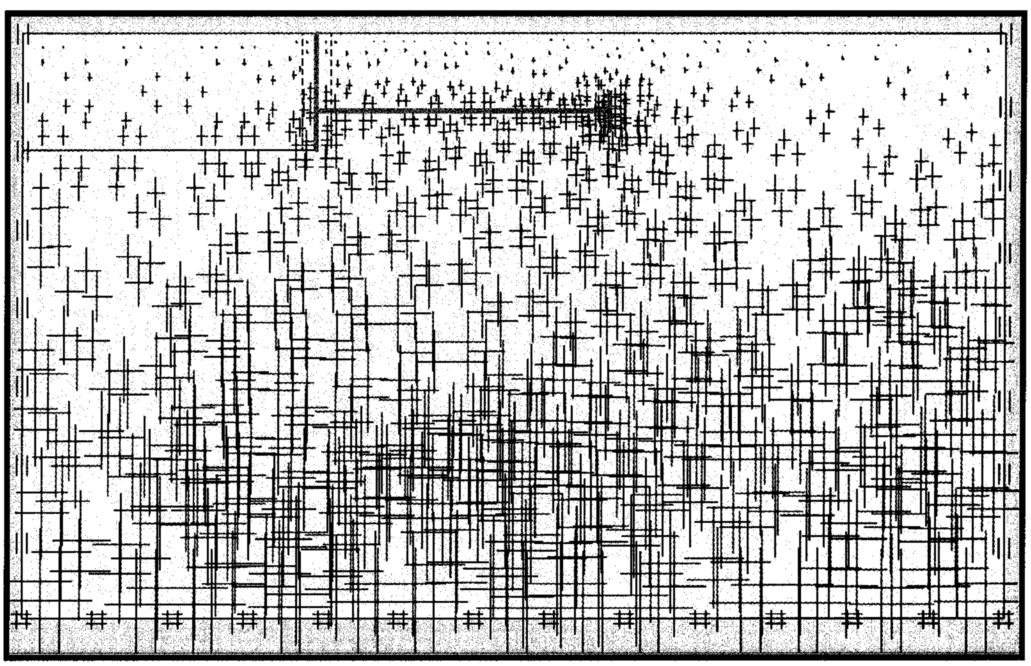

Figure 3.9 Initial stresses generated in model 2 with $\varphi = 30^0$ and OCR=2

In general, the initial effective stresses at a stress point (presented in figure 3.9) were obtained from the weight of the material above this point and the value of ∑Mweight. The equations were given as:

$$\sigma'_{v,o} = \sum Mweight\left(\sum_i \gamma_i h_i - P_w\right) \ldots\ldots\ldots\ldots\ldots\ldots\ldots\ldots\ldots\ldots\ldots\ldots (3.14)$$

$$\text{and } \sigma'_{h,o} = K_o \sigma'_{v,o} \ldots\ldots\ldots\ldots\ldots\ldots\ldots\ldots\ldots\ldots\ldots\ldots\ldots\ldots\ldots\ldots\ldots\ldots (3.15)$$

Where γ_i is the unit weight of individual layers; h_i is the layer depth and P_w is the initial pore pressure in the stress point. In present study the initial pore water pressure, PWP, was considered zero.

3.10 Staged Construction

In numerical analysis with finite element model, staged construction was the most important type of loading input to change in geometry and load configuration. Deactivating or reactivating loads, volume clusters or structural objects as created in the geometry input was possible during staged construction. It also provided an accurate and realistic simulation of various loading, construction and excavation processes.

3.10.1 Loading Increment

The entire loading increment during the staged construction was divided into three major phases for all three numerical models.

Phase 1 consisted of excavation of soil in front of the wall. At the same time replaced it by an equivalent triangular loading, which considered a value of $K_o \gamma H$ at the bottom of

the wall and 0 at the top surface. During this staged construction, the soil body was at-rest condition.

Phase 2 was developed by the installation of the concrete wall plate, and earth anchor (model with anchor plate screwed with vertical wall). Simultaneously, the triangular equivalent loading applied during phase 1 was deactivated. Still the soil body was considered in at-rest condition.

Phase 3 was the main stage to generate the passive earth condition on the retaining structure. It consisted of pushing the retaining wall towards the soil (for the model with retaining wall) or away from the soil (for the model with retaining wall and vertical anchor plate) with a uniform horizontal displacement to create a passive earth pressure. By several trials, the value of maximum displacement was determined to cause the soil body collapse.

Soil reaction against this maximum displacement and distributions of the passive earth pressure against the wall and the vertical embedded anchor plate were examined by a number of executions of the numerical models. The ultimate failure load (P_{ult}) was calculated using Chin (1972) method which is further discussed later in this chapter. This method of approximation, proposed by Chin (1972), was used to obtain the maximum possible passive earth pressure. By incorporating this ultimate failure load, the coefficient of passive earth pressure was calculated for different numerical models using the following formulae.

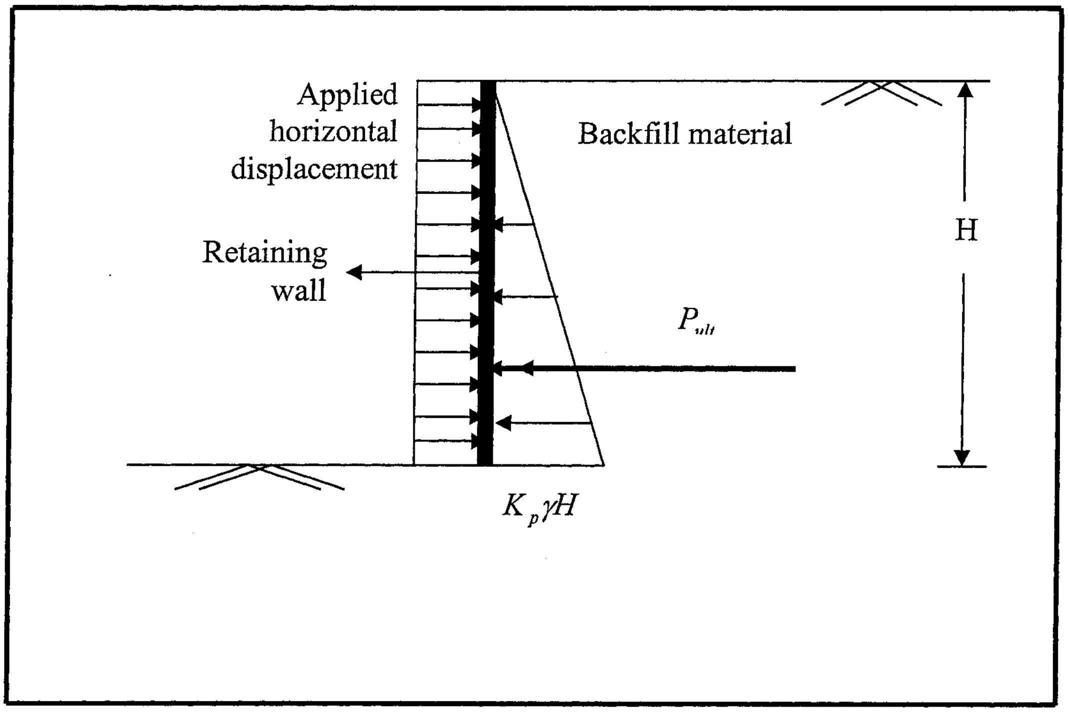

Figure 3.10 Passive earth pressure on retaining wall

The coefficient of passive earth pressure acting on vertical retaining wall, which was displaced horizontally towards the soil, can be calculated as:

$$K_p = \frac{P_{ult}}{\frac{1}{2}\gamma_s H^2} \quad \ldots (3.16)$$

Where, P_{ult} = ultimate failure load to create the maximum passive earth pressure (kN/m)

H = height of retaining wall (m)

γ_s = unit weight of backfill soil (kN/m^3)

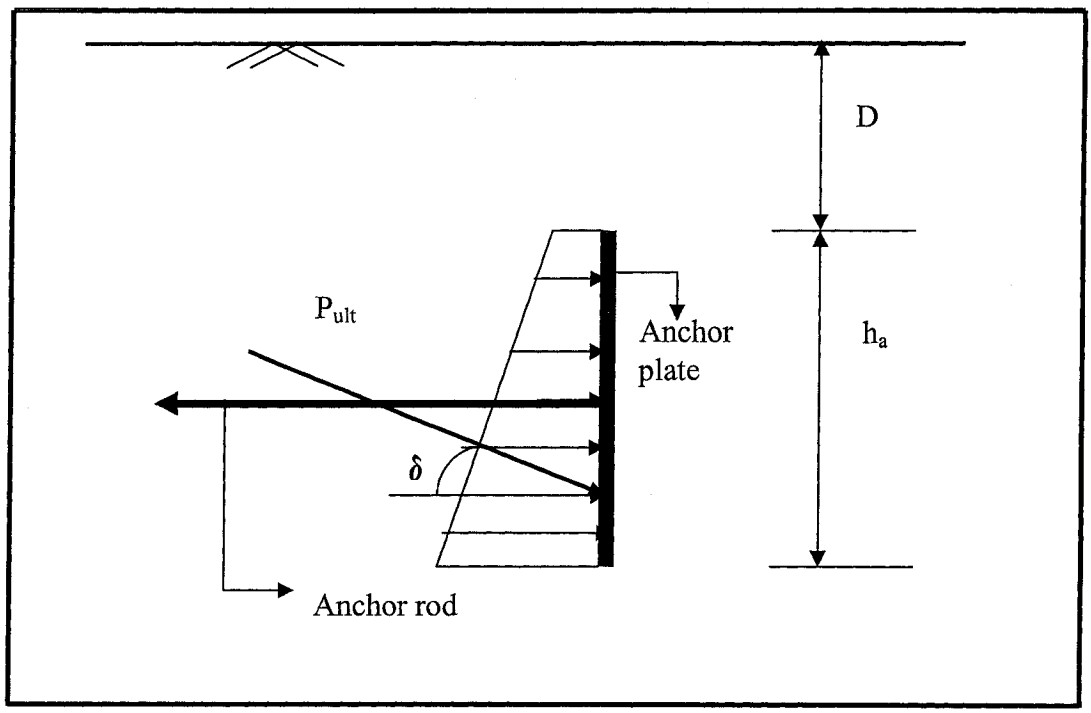

Figure 3.11 Distribution of passive earth pressure on an embedded anchor plate

For embedded anchor plate, coefficient of passive earth pressure was the function of depth of embedment, unit weight of backfill material and also the frictional angle between the anchor plate and surrounding soil body. Hence, K_p was calculated using the following expression:

$$K_p = \frac{P_{ult}}{\frac{1}{2} \times h_a \times \cos\delta \times (2 \times \gamma_s \times D + \gamma_s \times h_a)} \quad \ldots\ldots\ldots\ldots\ldots\ldots\ldots\ldots\ldots (3.17)$$

Where, h_a = height of anchor plate

D = depth of top of the anchor plate from the soil surface

δ = friction angle between soil and the anchor plate.

P_{ult} = ultimate load to create the maximum passive earth pressure

3.11 Variable Parameters

In present investigation using Mohr-Coulomb model, some parameters were kept isolated in order to determine their effects on K_p. Table 3.9 presents the summary of the range of some physical and mechanical characteristics of the sand and also some other factors that could really effect the passive earth pressure acting on the earth retaining structures.

Table 3.9 Physical and mechanical parameters considered in the numerical models

Parameters	Unit	Range
Angle of shearing resistance, ϕ	Degree, (^{0})	30^0 to 45^0
Unit weight of soil, γ	kN/m^3	16.5 to 19.5
Over consolidation ratio, OCR	-	1 to 4
Modulus of elasticity of soil, E	kN/m^2	Proposed chart (section 3.5)
Height of the retaining wall, H	m	6 to 12
Embedded depth of anchor plate, D	m	0 to 8

The unit weight of soil γ was constant for each value of ϕ. A relation between E and OCR was proposed to consider the effect of OCR in the initial effective stresses. Height of the retaining wall was changed to investigate the effect of embedded depth on the anchor plate in model 2. The position of the anchor plate changed with the changing height of retaining wall and thus variable depth of embedment was obtained.

3.12 Validation of the Numerical Model with Test Results

In order to validate the numerical models developed in the present investigation, the experimental data presented by Hanna and Khoury (2005) was considered. The objective of this comparative study was not only to validate the numerical models developed by finite element method but also to establish the experimental work performed by Hanna and Khoury (2005). This study also provided a strong background against the design charts and empirical formulae proposed on the basis of experimental work. Two sets of numerical model with retaining wall were developed. One model was for homogeneous cohesionless backfill and another for overconsolidated backfill overlying natural deposit. Numerical model used in this section was developed and analyzed by introducing the same parameters (presented in table 3.10), boundary conditions and the dimension of the retaining wall considered in experimental model by Hanna and Khoury (2005). This section will illustrate only the results obtained from homogeneous backfill. Table 3.10 presents the variable parameters considered in the experimental model.

Table 3.10 Variable parameters considered in the experimental model by Hanna & Khoury (2005)

Test Number	Sand Condition	Relative density D_r (%)	Unit Weight γ (kN/m^3)	ϕ, (degree)	wall friction δ (degree)	OCR
1	Loose	21	17.75	33	15	1.3
2	Medium	52	18.65	40	18	2.0
3	Dense	75	19.25	45	20	2.5

Comparison between the two results obtained from the laboratory experiment (Hanna and Khoury, 2005) and the numerical model (present investigation) are presented in table 3.11.

Table 3.11 Comparison between experimental results (Hanna and Khoury, 2005) and numerical model (present study)

Test Number	Angle of shearing resistance ϕ (degree)	Over consolidation ratio	$K_{p(oc)}$ Hanna and Khoury (2005)	$K_{p(oc)}$ Present investigation
1	33	1.3	8.15	8.78
2	40	2.0	14.92	14.01
3	45	2.5	22.45	18.7

Figure 3.12 presents the graphical representation of the results obtained from two different studies. For loose and medium dense sand ($\phi = 33^0$ and 40^0), the numerical model provided a very good agreement with the experimental results where as for heavily dense sand ($\phi = 45^0$ and OCR=2.5), the values of K_p was relatively lower compared to the experimental value. This could be due to the fact that the Mohr-Coulomb model was less sensitive to OCR compared to other variable parameters. There was no option to introduce the value of OCR directly in the finite element model as an input data rather it was expressed in terms of K_o. Thus at relatively higher OCR, the numerical model might provide a conservative value.

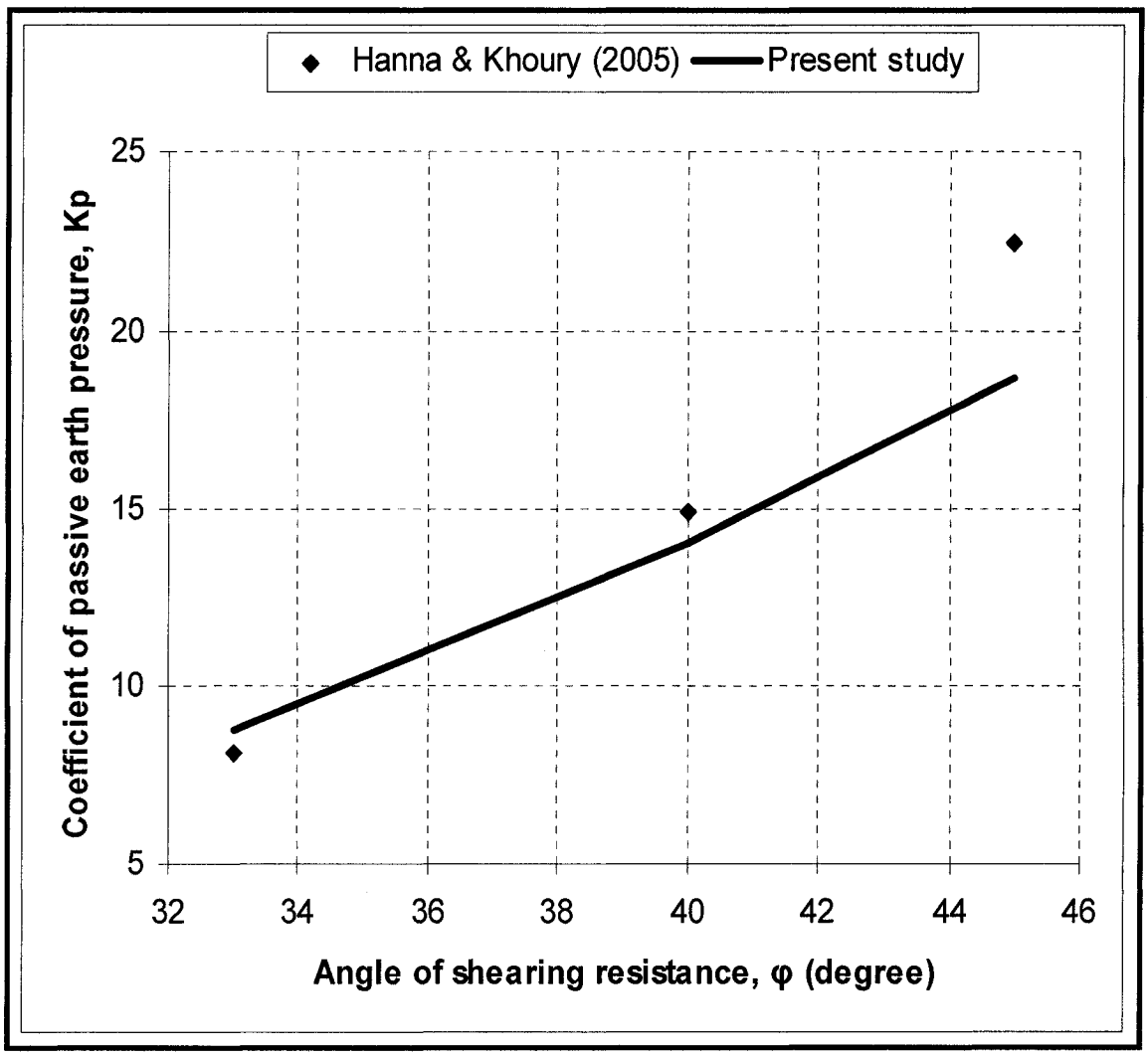

Figure 3.12 Variation of K_p with angle of shearing resistance, φ for comparative study

3.13 Numerical Analysis of Embedded Anchor Plate

In present investigation, the second numerical model with vertical anchor plate screwed with a rigid wall was analyzed to examine the effects of various physical and elastic parameters of backfill materials. The model was further investigated to determine the effect of overburden on the passive earth pressure acting on the embedded anchor plate at different soil condition. Both normally and over consolidated soil conditions were considered to investigate the effect of OCR on K_p which was the prime factor to design the anchor plate. The present testing program was divided into two different groups for both normally consolidated and over consolidated $(1 \leq OCR \leq 4)$ soil. Both sands correspond to different ϕ were further investigated for different embedded depth of the anchor plate. Then, for a fixed value of ϕ, μ, D and δ/ϕ, the passive earth pressure was investigated for different OCR.

3.13.1 Effect of Angle of Shearing Resistance, ϕ

Angle of shearing resistance had a great influence on the passive earth pressure within the soil body. In present investigation, four different states of cohesionless materials were used. The values of friction angles, ϕ, for backfill materials were considered as 30^0, 35^0, 40^0 and 45^0 (i.e. loose, medium, medium dense and dense sand). For a fixed embedded depth of an anchor plate, the OCR varied from 1 to 4, δ/ϕ=1/3 and Poisson's ratio μ=0.3 was considered.

Finally the following variation (figure 3.13) of $K_{p(oc)}$ with ϕ was calculated (using equation 3.17) from the ultimate failure loads. This failure load was obtained from different load-displacement curves at different OCR.

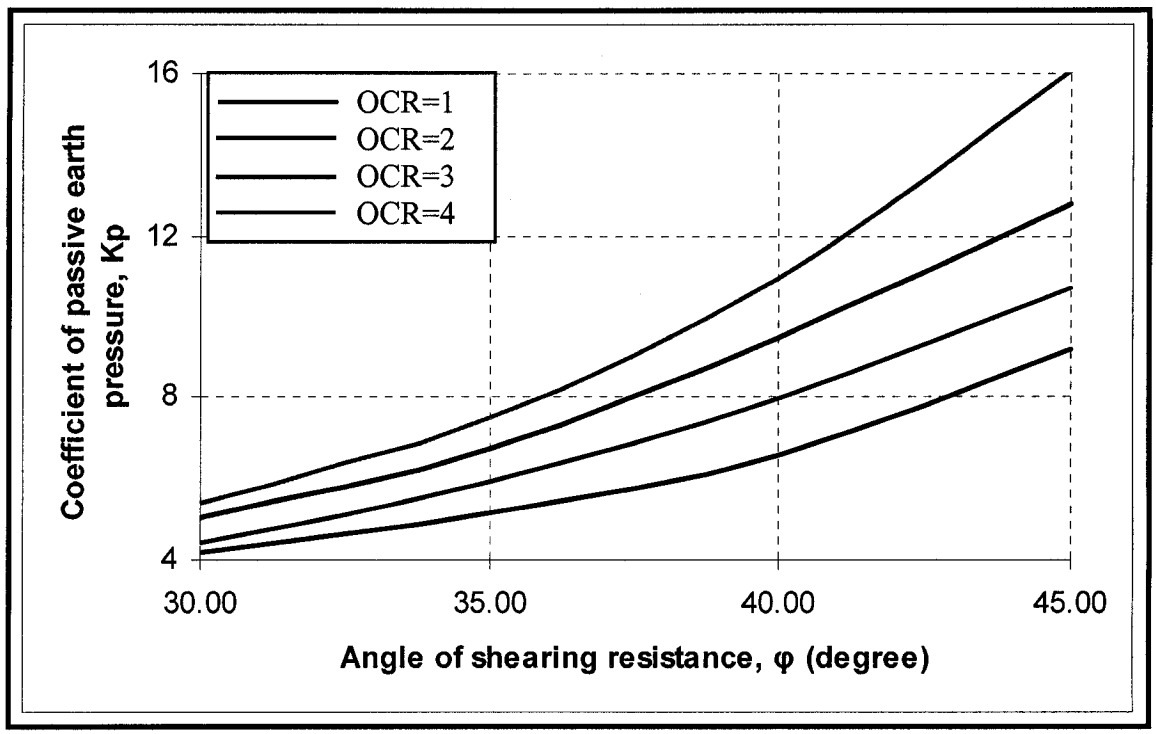

Figure 3.13 Variation of K_p with angle of shearing resistance, φ at different OCR

From figure 3.13, it could be concluded that the value of the passive earth pressure in front of an embedded anchor plate increases with increasing the angle of shearing resistance within the surrounding soil body. This trend was constant for different OCR within the soil. This type of variation resulted due to the fact that, when the soil was in denser condition, it could resist much higher lateral earth pressure compared to that of loose soil and thus the ultimate failure load was much higher for dense state condition. As the coefficient of passive earth pressure was the function of this ultimate failure load, the increase in φ lead to an increase of coefficient of passive earth pressure.

3.13.2 Effect of Overconsolidation Ratio, (OCR)

Overconsolidation ratio, defined as the ratio of the maximum vertical effective stress over the actual vertical effective stress ($\sigma'_{v\max} / \sigma'_v$), was one of the most significant parameters of the soil that could really change the values of $K_{p(oc)}$ for different friction angles. Figure 3.14 presents a typical plot of $K_{p(oc)}$ against OCR at different frictional angle, φ.

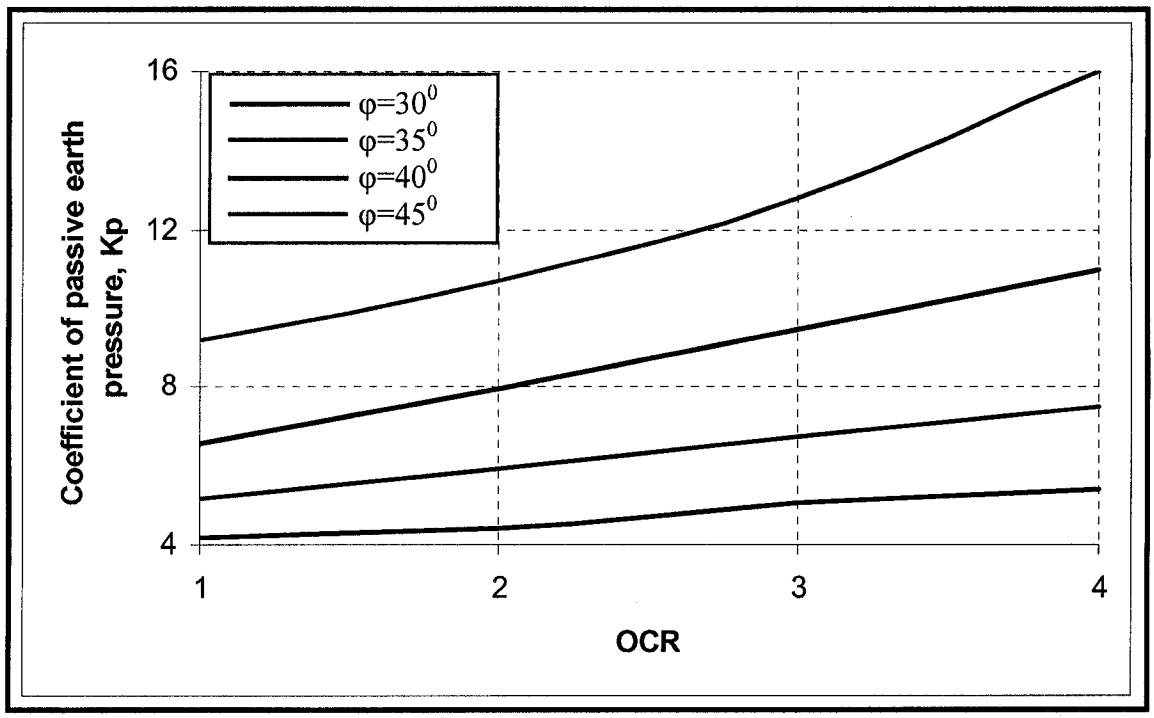

Figure 3.14 Variation of K_p with OCR at different angle of shearing resistance, φ

The above figure shows that the K_p value increases due to the increase in OCR. This was due to the fact that a portion of the effective horizontal pressure, developed during the initial loading, remained within the soil while the effective vertical stress was reduced and a stiffer compacted soil resulted. This mechanism of stress created a dense condition within the soil body and thus the passive earth pressure increased.

3.13.3 Effects of Overburden

The overburden pressure on an embedded earth structure may be either in the form of applied surcharge on the backfill material or the self weight of the backfill soil or the both. To design an earth anchor, the embedded depth of the anchor plate and the vertical overburden pressure (with or without surcharge) is an important consideration. This is due to the fact that the overburden can enormously affect the passive earth pressure acting on an anchor plate. In present investigation, the analysis with numerical model was performed to examine the change of passive earth pressure with increasing depth of embedment as well as to compare these values with those obtained for vertical retaining wall. A markable variation of passive earth pressure was observed with different embedded depths presented in table 3.12, 3.13, 3.14, and 3.15 in terms of K_p. The passive earth pressure acting on the anchor plate was also found different from those acting on retaining wall under different soil conditions.

Table 3.12 K_P values behind a retaining wall & an anchor plate ($\phi = 30^0$)

Height of the anchor plate, h_a = 2m

Poisson's ratio, μ = 0.3,

Wall and plate friction, δ/ϕ = 1/3

ϕ (degree)	OCR	Height of the retaining wall, H (m)	Embedded depth of the anchor plate, D (m)	K_p on retaining wall	K_p on anchor plate
30	2	2.00	0.00	7.00	7.00
		6.00	3.00	7.00	4.41
		8.00	4.33	7.00	3.99
		10.00	5.67	7.00	3.78
		12.00	8.00	7.00	3.5
	3	2.00	0.00	8.00	8.00
		6.00	3.00	8.00	5.04
		8.00	4.33	8.00	4.72
		10.00	5.67	8.00	4.40
		12.00	8.00	8.00	4.16
	4	2.00	0.00	9.00	9.00
		6.00	3.00	9.00	5.4
		8.00	4.33	9.00	4.95
		10.00	5.67	9.00	4.77
		12.00	8.00	9.00	4.5

Table 3.13 K_P values behind a retaining wall & an anchor plate (ϕ= 35^0)

Height of the anchor plate, h_a = 2m

Poisson's ratio, μ = 0.3,

Wall and plate friction, δ/ϕ = 1/3

ϕ (degree)	OCR	Height of the retaining wall, H (m)	Embedded depth of the anchor plate, D (m)	K_p on a retaining wall	K_p on an anchor plate
35	2	2.00	0.00	9.00	9.00
		6.00	3.00	9.00	5.94
		8.00	4.33	9.00	5.4
		10.00	5.67	9.00	4.95
		12.00	8.00	9.00	4.77
	3	2.00	0.00	10.00	10.00
		6.00	3.00	10.00	6.80
		8.00	4.33	10.00	6.30
		10.00	5.67	10.00	5.70
		12.00	8.00	10.00	5.30
	4	2.00	0.00	11.00	11.00
		6.00	3.00	11.00	7.48
		8.00	4.33	11.00	6.71
		10.00	5.67	11.00	6.05
		12.00	8.00	11.00	5.83

Table 3.14 K_P values behind a retaining wall & an anchor plate ($\phi = 40^0$)

Height of the anchor plate, h_a = 2m

Poisson's ratio, μ = 0.3,

Wall and plate friction, δ/ϕ = 1/3

ϕ (degree)	OCR	Height of the retaining wall, H (m)	Embedded depth of the anchor plate, D (m)	K_p on a retaining wall	K_p on an anchor plate
40	2	2.00	0.00	11.75	11.75
		6.00	3.00	11.75	7.99
		8.00	4.33	11.75	7.76
		10.00	5.67	11.75	7.05
		12.00	8.00	11.75	6.93
	3	2.00	0.00	13.5	13.5
		6.00	3.00	13.5	9.45
		8.00	4.33	13.5	9.18
		10.00	5.67	13.5	8.51
		12.00	8.00	13.5	7.83
	4	2.00	0.00	15.00	15.00
		6.00	3.00	15.00	10.95
		8.00	4.33	15.00	10.05
		10.00	5.67	15.00	8.85
		12.00	8.00	15.00	8.25

Table 3.15 K_P values behind a retaining wall & an anchor plate ($\phi = 45^0$)

Height of the anchor plate, h_a = 2m

Poisson's ratio, μ = 0.3,

Wall and plate friction, δ/ϕ = 1/3

ϕ (degree)	OCR	Height of the retaining wall, H (m)	Embedded depth of the anchor plate, D (m)	K_p on a retaining wall	K_p on an anchor plate
45	2	2.00	0.00	15.00	15.00
		6.00	3.00	15.00	10.65
		8.00	4.33	15.00	10.5
		10.00	5.67	15.00	10.35
		12.00	8.00	15.00	10.05
	3	2.00	0.00	17.50	17.50
		6.00	3.00	17.50	12.78
		8.00	4.33	17.50	12.43
		10.00	5.67	17.50	11.90
		12.00	8.00	17.50	10.85
	4	2.00	0.00	19.25	19.25
		6.00	3.00	19.25	15.98
		8.00	4.33	19.25	13.67
		10.00	5.67	19.25	12.90
		12.00	8.00	19.25	11.74

It is quite obvious from the above tables that an increase in overburden caused decrease in the passive earth pressure acting on the embedded anchor plate for different friction angle, ϕ and OCR. These tables also indicate that the passive earth pressure on an embedded anchor was always lower compared to the passive pressure acting on vertical wall. This variation of the passive earth on anchor could be the result of the following reasons:

1. In actual practice, the anchor rod is normally placed at the middle of the plate. The location of anchor rod might cause an eccentricity due to the earth pressure distribution in front of the embedded anchor plate when the displacement was applied. The center of gravity of the distributed passive pressure approached near the middle of the anchor plate with increasing embedded depth. As a result, the zone of passive decreased and active zone increased due to the pull out of the plate. Thus the passive earth pressure decreased with increasing overburden.

   Figure 3.15 (a) and 3.15(b) explain the location of center of gravity (CG) of resultant force at lower and relatively higher embedded depth. It also illustrates how the zone of passive pressure changes with changing CG at different depth of embedment.

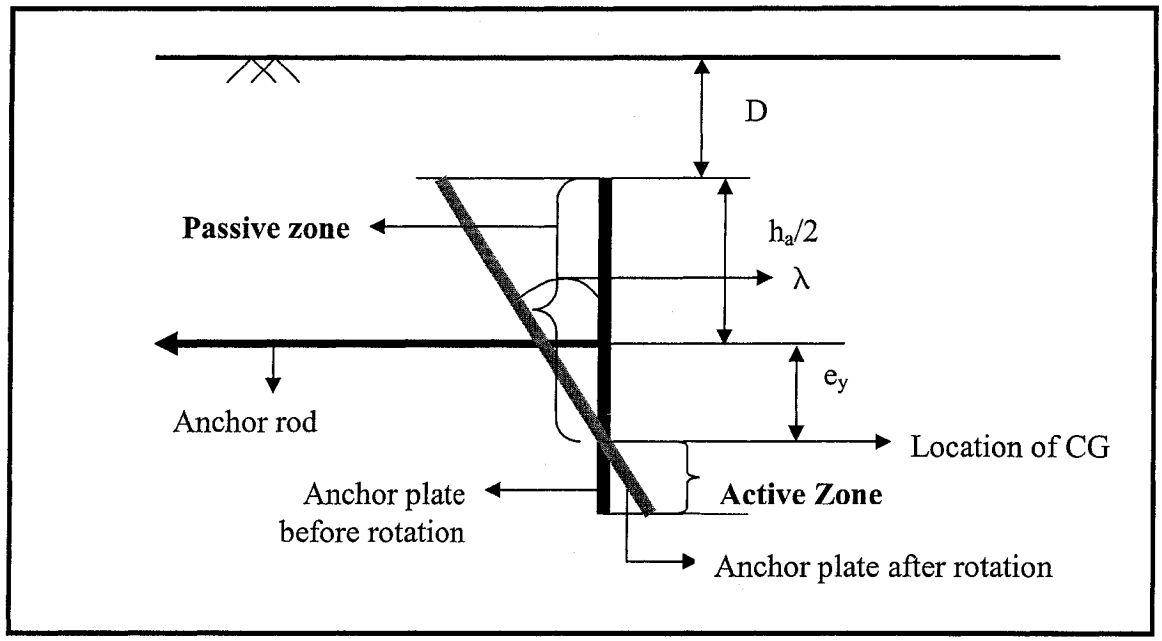

Figure 3.15(a) Location of CG and passive zone with small depth of embedment, D and higher eccentricity

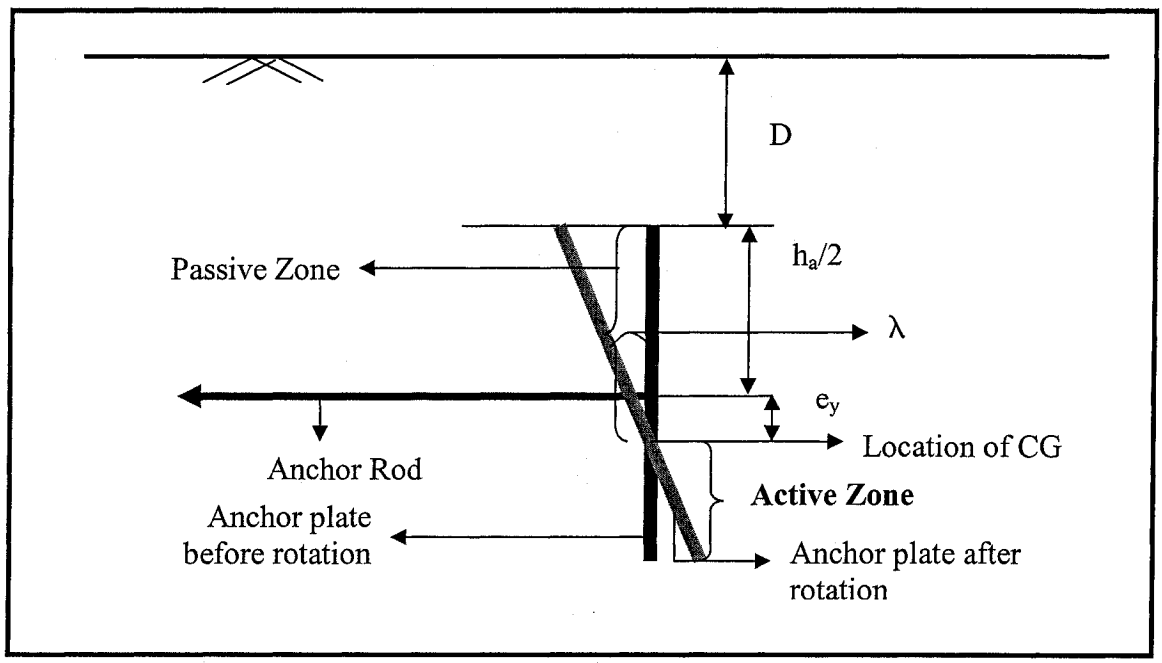

Figure 3.15(b) Location of CG and passive zone with large depth of embedment, D and lower eccentricity

In present study, several trials were made to investigate the effect of embedment on the location of center of gravity as well as the eccentricity. Table 3.16 shows the location of center of gravity and the eccentricity with increasing embedded depth in numerical model.

Table 3.16 Location of center of gravity and the eccentricity with increasing depth

Depth of embedment, D (m)	Location of center of gravity from the bottom of the plate (m)	Eccentricity, e_y (fig 3.16) (m)
0.00	0.6667	0.3333
3.00	0.9167	0.0833
4.33	0.9375	0.0625
5.67	0.9500	0.04999
8.00	0.9630	0.0370

Angle of rotation of the anchor plate, λ, against its center of gravity occurred due to the eccentricity of the resultant earth pressure. This rotational displacement of plate might cause the reduction in passive earth pressure on anchor.

For a fixed elevation, the passive earth pressure decreased with increasing rotational angle of the anchor plate. According to Caquot and Kerisel (1948),

$$K_p^{'} = R \times K_p \quad \dots \dots \dots \dots \dots \dots \dots \dots \dots \dots \dots \dots \dots \dots \dots \dots \quad (3.18)$$

Where, $K_p^{'}$ = coefficient of passive earth pressure on an inclined retaining wall.

R = reduction factor (Normally R<1)

K_p = coefficient of passive earth pressure behind a vertical retaining wall.

They also proposed a design chart of reduction factor, R, against the inclination of the vertical retaining wall, α for different frictional angle, ϕ. In the present study, the rotational angle λ was found to be the only function of the embedded depth and was not dependent on the elastic properties and stress condition of the backfill soil. Table 3.17 and 3.18 show that the values of λ were constant for different ϕ and OCR but it decreased with increasing overburden as the eccentricity of the resultant force approached to zero.

Table 3.17 Rotational angle of anchor plate at different embedded depth at ϕ=30^0 and OCR=1

ϕ (degree)	OCR	γ (kN/m^3)	Depth of embedment D (m)	λ (degree)
30	1	16.5	3.00	63.9
			4.33	62.6
			5.67	61.9
			8.00	57.3

Table 3.18 Rotational angle of anchor plate at different embedded depth at ϕ=45^0 and OCR=2

ϕ (degree)	OCR	γ (kN/m^3)	Depth of embedment D (m)	λ (degree)
45	2	19.5	3.00	63.9
			4.33	62.6
			5.67	61.9
			8.00	57.3

In spite of decreasing λ, the value of passive pressure on the anchor plate decreased. This was just because the effective passive pressure zone on anchor plate was gradually decreasing with increasing depth of embedment as the eccentricity of the resultant earth pressure approached to zero.

2. For an embedded anchor plate, ultimate failure load was the function of both passive earth pressure as well as the overburden pressure caused by the self-weight of the backfill material.

$$P_{ult} = \frac{1}{2} K_p \gamma h_a^2 + K_q \gamma D h_a \ldots\ldots\ldots\ldots\ldots\ldots\ldots\ldots\ldots\ldots (3.19)$$

Where, $K_q = \dfrac{K_p}{\cos(\beta - \lambda)}$

For horizontal earth surface, $\beta = 0$ and $K_q = \dfrac{K_p}{\cos\lambda}$. With increasing depth of embedment, K_q decreased due to the decrease in λ. Thus a reduced value of passive pressure was obtained by using equation 3.19 with increasing overburden, D.

From this numerical model analysis with anchor plate, it is quite obvious that the passive earth pressure on an embedded anchor plate was relatively lower compared to that obtained for the retaining wall under any soil condition. So, the design of an anchor considering the same passive pressure as wall may result an unsafe retaining structure. In present investigation, a reduction factor (discussed later in this chapter) was proposed to calculate the actual passive earth pressure on anchor plate.

3.14 Numerical Model of Retaining Wall in Overconsolidated Backfill Overlying Natural Deposit

In actual field condition, the anchor plates are not embedded in homogeneous backfill material. After excavating a certain depth in the ground, the anchor is placed and the vertical cut is then refilled with backfill material. Normally the backfill material is compacted at a certain level by keeping the soil below the anchor plate undisturbed. The results obtained from previous two numerical models with homogeneous soil concluded that a reduction factor should be introduced to calculate the passive earth pressure on embedded anchor. So, the design charts and formulae proposed by Hanna and Khoury (2005) for retaining wall can be used to calculate the earth pressure on anchor by multiplying with reduction factor. The numerical model analysis of retaining wall in overconsolidated backfill overlying natural deposit was performed to compare the values of passive earth pressure with the experimental works performed by Hanna and Khoury (2005). If this numerical model supports the design formula developed on the basis of their experimental works on overlayer soil case, it can be concluded that the same reduction factor can be considered to calculate the passive pressure on embedded anchor in layered soil.

To develop this numerical model, all basic parameters of soil, initial stress conditions, boundary conditions and the load increment during staged constructions were considered as the same used in the numerical model with homogeneous backfill.

The parameters considered in the experimental investigation by Hanna and Khoury (2005) are presented in table 3.19. Comparison between their experimental works and the numerical analysis is presented in table 3.20.

Table 3.19 Parameters used in experimental investigation by Hanna and Khoury (2005) case of backfill overlying deposit

Test number	Sand Condition	Relative density D_r (%)	Unit Weight γ (kN/m^3)	ϕ (degree)	wall friction δ (degree)	OCR
4	Dense/Medium	75/52	19.25/18.65	45/40	20	2.2
5	Medium/Dense	52/75	18.65/19.25	40/45	18	2.3

Table 3.20 Comparison between experimental results (Hanna & Khoury, 2005) & numerical model (present study) case of backfill overlying deposit

Test number	Angle of shearing resistance ϕ (degree)	Over consolidation ratio	$K_{p(oc)}$ Hanna and Khoury (2005)	$K_{p(oc)}$ Present investigation
4	45/40	2.2	19.30	20.41
5	40/45	2.3	18.70	15.60

The values of coefficient of passive earth pressure on retaining wall obtained from the numerical analysis provided a very good agreement with the experimental works by Hanna and Khoury (2005). On the basis of their experimental investigation, Hanna and Khoury proposed an analytical formula for the strong overconsolidated cohesionless backfill overlying a weak natural deposit which can be expressed as:

$$K_p\left(\frac{backfill}{deposit}\right)=\left[\frac{K_p(backfill)+K_p(deposit)}{2}\right] \quad \ldots\ldots\ldots\ldots\ldots\ldots\ldots\ldots (3.20)$$

Where, $K_p(backfill)$= Coefficient of passive earth pressure of homogeneous backfill material

$K_p(deposit)$ = Coefficient of passive earth pressure for the homogeneous lower deposit

The value of $K_p(backfill)$ and $K_p(deposit)$ can be calculated either using the formula,

$$P_{p(oc)} = \frac{P_{rm} + \sum w \tan(\alpha + \phi)}{1 - \tan\delta \tan(\alpha_w + \phi)} \quad \ldots\ldots\ldots\ldots\ldots\ldots\ldots\ldots\ldots\ldots\ldots\ldots\ldots \quad (3.21)$$

$$\text{Where, } K_{p(oc)} = \frac{2P_{p(oc)}}{\gamma h^2 d}$$

or an empirical formulas proposed by Hanna and Khoury (2005) for rough retaining wall where (1/2<δ/ϕ<2/3).

$$K_{p(oc)} = K_{p(nc)}\left\{1.5 - \left(\frac{\delta - 25}{100}\right)\right\}\{OCR\}^{\sin\delta} \quad \ldots\ldots\ldots\ldots\ldots\ldots\ldots\ldots \quad (3.22)$$

or from the design charts proposed by Hanna and Khoury (2005).

The empirical formula presented in equation 3.20 was only validated with the test results due to the lack of experimental and field data. So, further analysis with this numerical model was conducted to establish the formula presented in equation 3.20.

Figure 3.16 and 3.17 show the variation of K_p in experimental work and numerical model on a retaining wall if the backfill material is strong and overconsolidated compared to the underneath natural deposit. In laboratory, K_p values of backfill and deposit materials were calculated using the design charts proposed by Hanna and Khoury (2005) for homogeneous backfill and incorporated these values in equation 3.20.

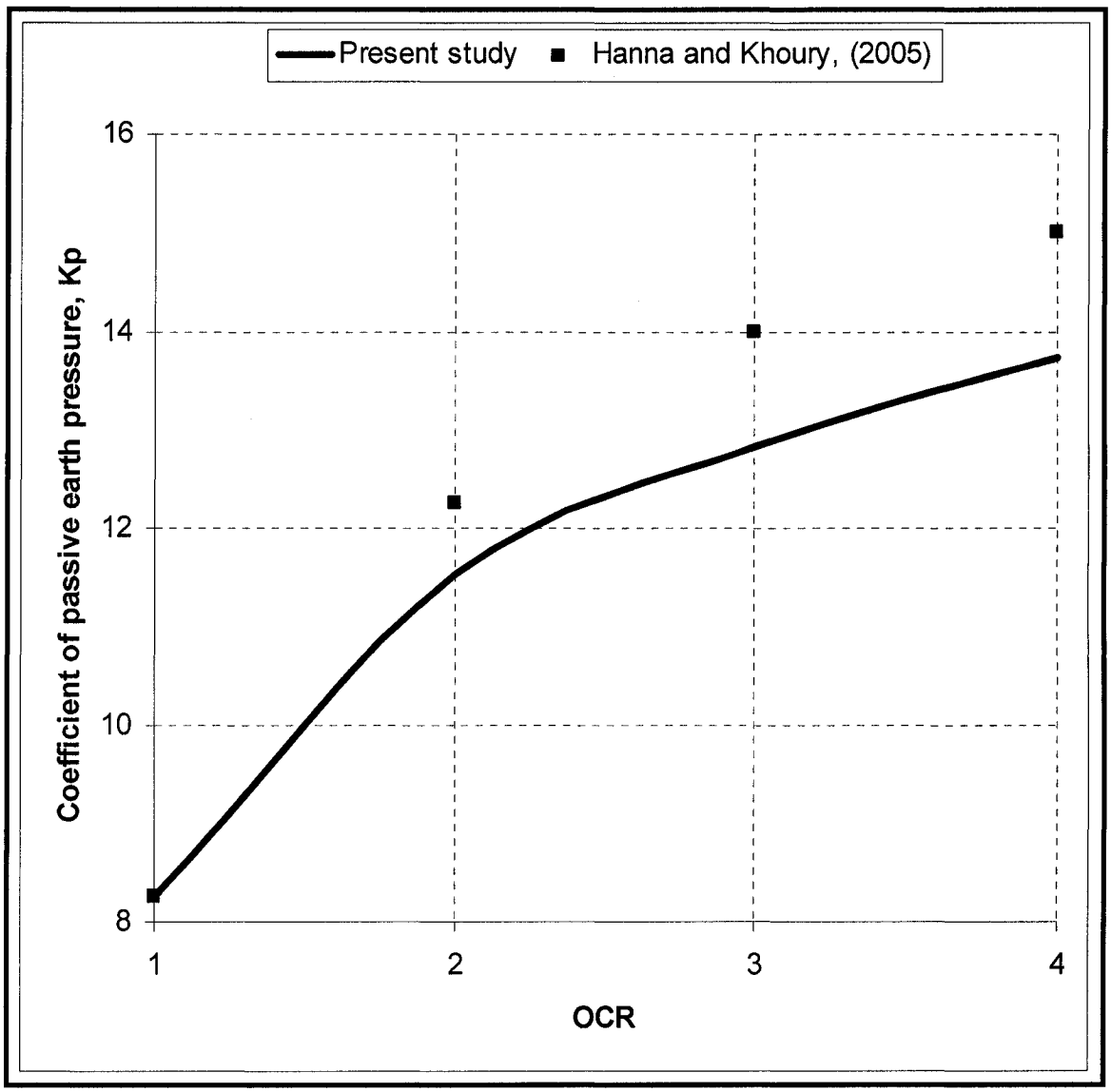

Figure 3.16 Variation of K_p with OCR for strong backfill (dense, $\varphi=45^0$) overlying weak deposit (medium dense, $\varphi=40^0$)

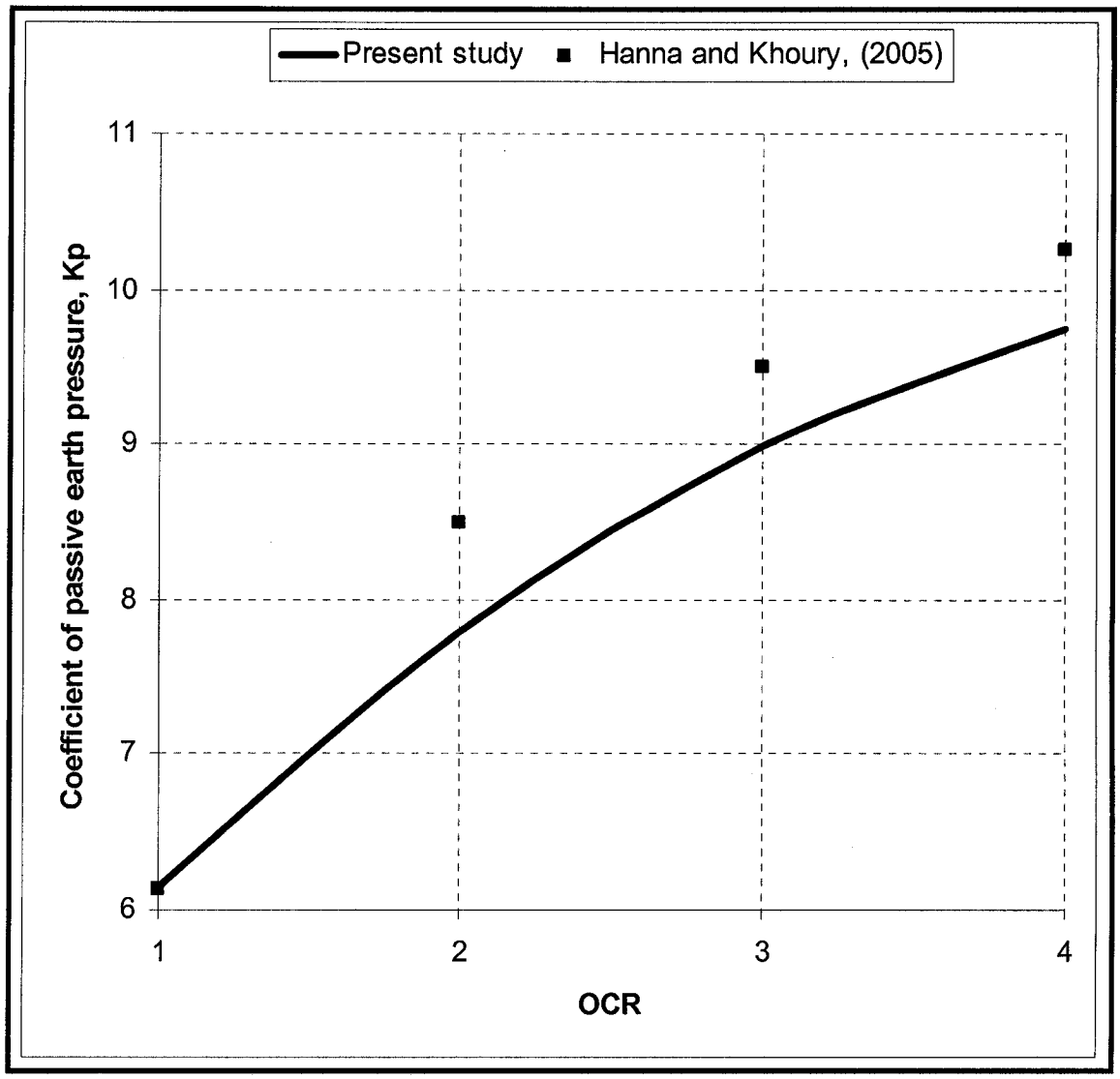

Figure 3.17 Variation of K_p with OCR for strong backfill (medium dense, $\varphi=40^0$) overlying weak deposit (medium, $\varphi=35^0$)

Variation of the results obtained from the analytical formula proposed by Hanna and Khoury (2005) and the numerical analysis in the present study ranged from 9% to 20% (<25%) at higher OCR. At lower OCR, the results were quite similar. So, it can be concluded that the proposed formulation for K_p by Hanna and Khoury (2005) in an overlayer soil case was well able to estimate the passive earth pressure on a retaining wall as well as on a vertical anchor plate by multiplying the values with reduction factor.

3.15 Design of Embedded Vertical Anchor

Earth retaining structure that derives its stability from the anchor plates is basically designed for the ultimate load carrying capacity and the displacement of the anchor plate. In present study, two analytical formulae had been developed to calculate the failure load carried out by anchor plate and its displacement at any arbitrary load. This section will illustrate the step by step procedure to calculate the proposed ultimate load and an arbitrary displacement to design an anchor plate. Finally a design procedure is proposed based on these proposed formulae.

3.15.1 Proposed Formulae for Vertical Anchor Plate

The system with anchor plate is different from the conventional tied back system. There are several major conditions that are pertinent to the proper design and analyze the total system. (1) The calculation of the anchor plates resistance capacity. (2) The initial stability analysis of the system. (3) Determination of the magnitude and distribution of lateral earth pressure on the vertical plate.

3.15.1.1 Mathematical formulation for ultimate failure load

Based on the numerical analysis discussed in previous sections (3.13), the following mathematical formulate is proposed to calculate the ultimate failure load. This failure load normally occurred when an embedded anchor plate was in maximum passive condition.

$$P_{ult} = \frac{1}{2} K_p \gamma H_{CG}^2 + K_q \gamma D H_{CG} \quad \text{...(3.23)}$$

Where,

$$H_{CG} = \frac{h_a}{2} + e_y \quad \text{...(3.23.1)}$$

$$K_{p(oc)} = R \times K_{p(nc)} \left\{ 1.5 - \left(\frac{\delta - 25}{100} \right) \right\} (OCR)^{\sin \delta} \quad \ldots\ldots\ldots\ldots\ldots\ldots\ldots (3.23.2)$$

Here, $K_{p(nc)anchor} = K_{p(nc)retainingwall}$ as R = 1 for any ϕ and OCR = 1

$$K_q = \frac{K_p}{\cos \lambda} \quad \ldots\ldots\ldots\ldots\ldots\ldots\ldots\ldots\ldots\ldots\ldots\ldots\ldots\ldots\ldots\ldots\ldots\ldots (3.23.3)$$

To determine the location of the resulting earth pressure, H_{CG}, determination of eccentricity e_y was a must. For a given height of the anchor plate and embedded depth, e_y could be calculated either by using the following formula or by the chart presented in figure. 3.18:

$$e_y = \left[\frac{Dh_a + \frac{1}{3}h_a^2}{2D + h_a} \right] \quad \ldots\ldots\ldots\ldots\ldots\ldots\ldots\ldots\ldots\ldots\ldots\ldots\ldots\ldots\ldots\ldots (3.24)$$

Once e_y is calculated, H_{CG} can be determined using the formula (3.23.1).

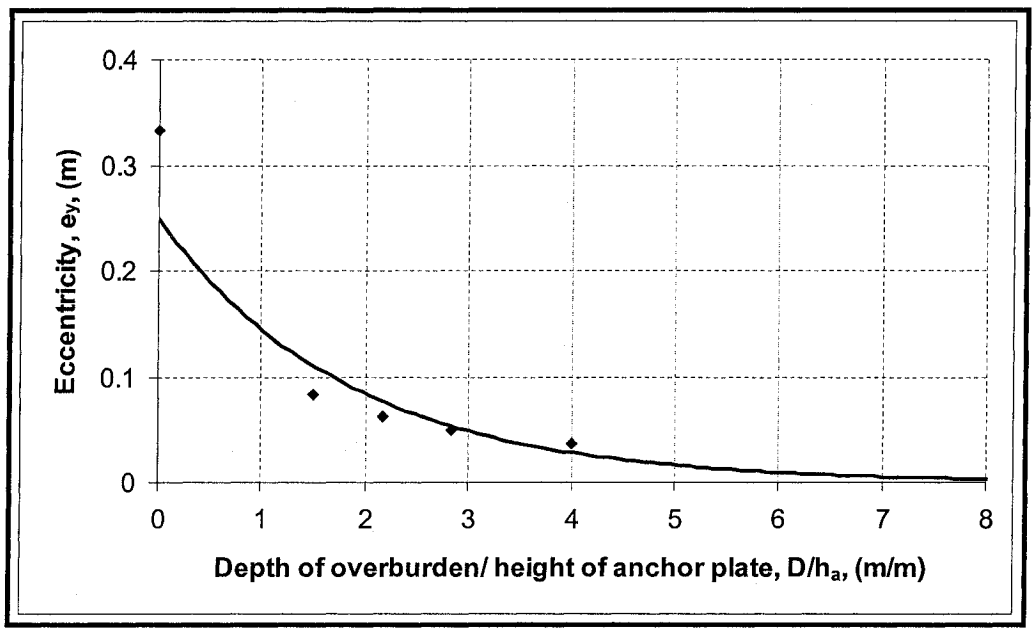

Figure 3.18 Eccentricity Vs depth/height ratio of vertical anchor plate in numerical model

The term reduction factor was introduced in the proposed formula due to the fact that the values of passive pressure in front of embedded anchor plate obtained from the numerical model were relatively lower than those of retaining wall at different shearing resistance, φ and OCR. Based on the results presented in tables 3.12, 3.13, 3.14, and 3.15 in section 3.13.3, the following design charts (figure 3.19, 3.20, 3.21) for reduction factor were proposed to calculate the values of $K_{p(oc)}$ in order to design of an anchor plate under passive condition.

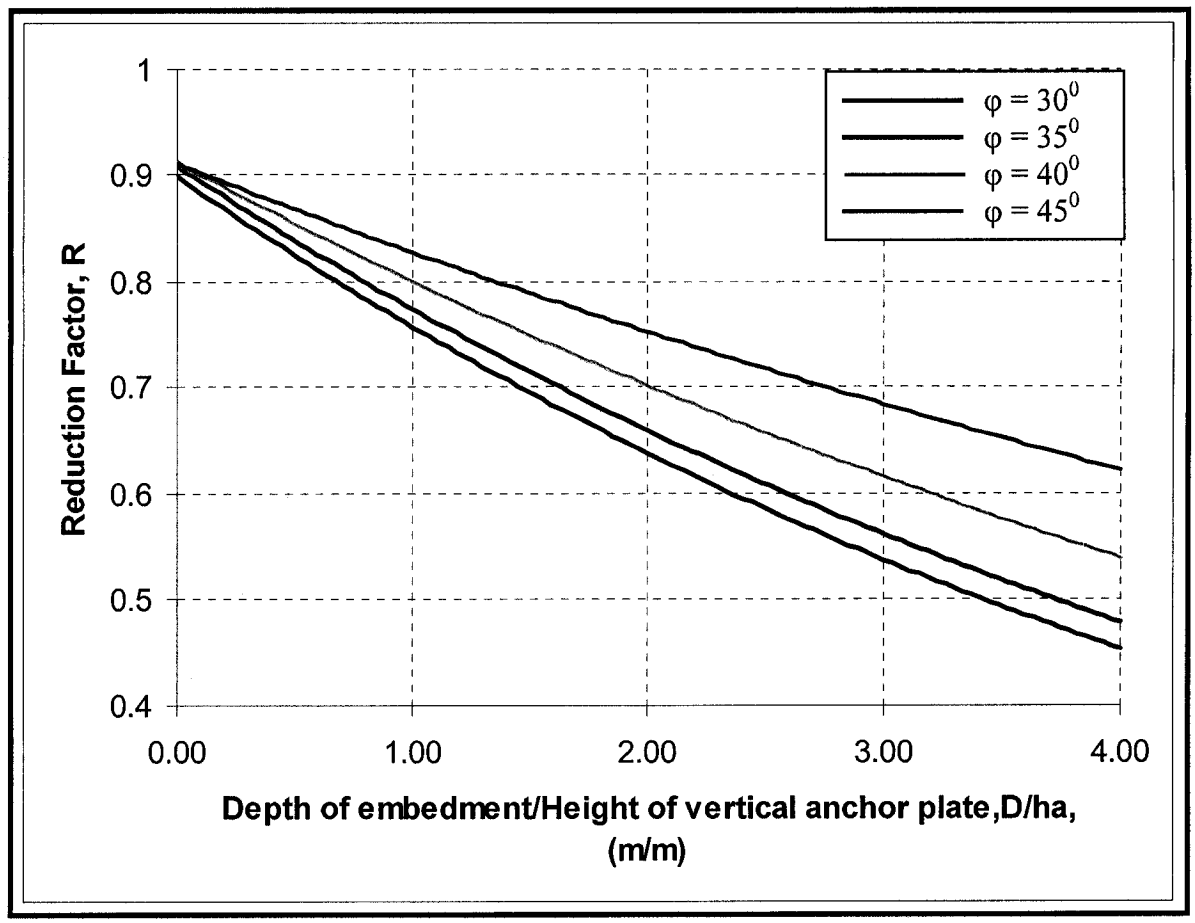

Figure 3.19 Proposed design charts for reduction factor, R at OCR=2

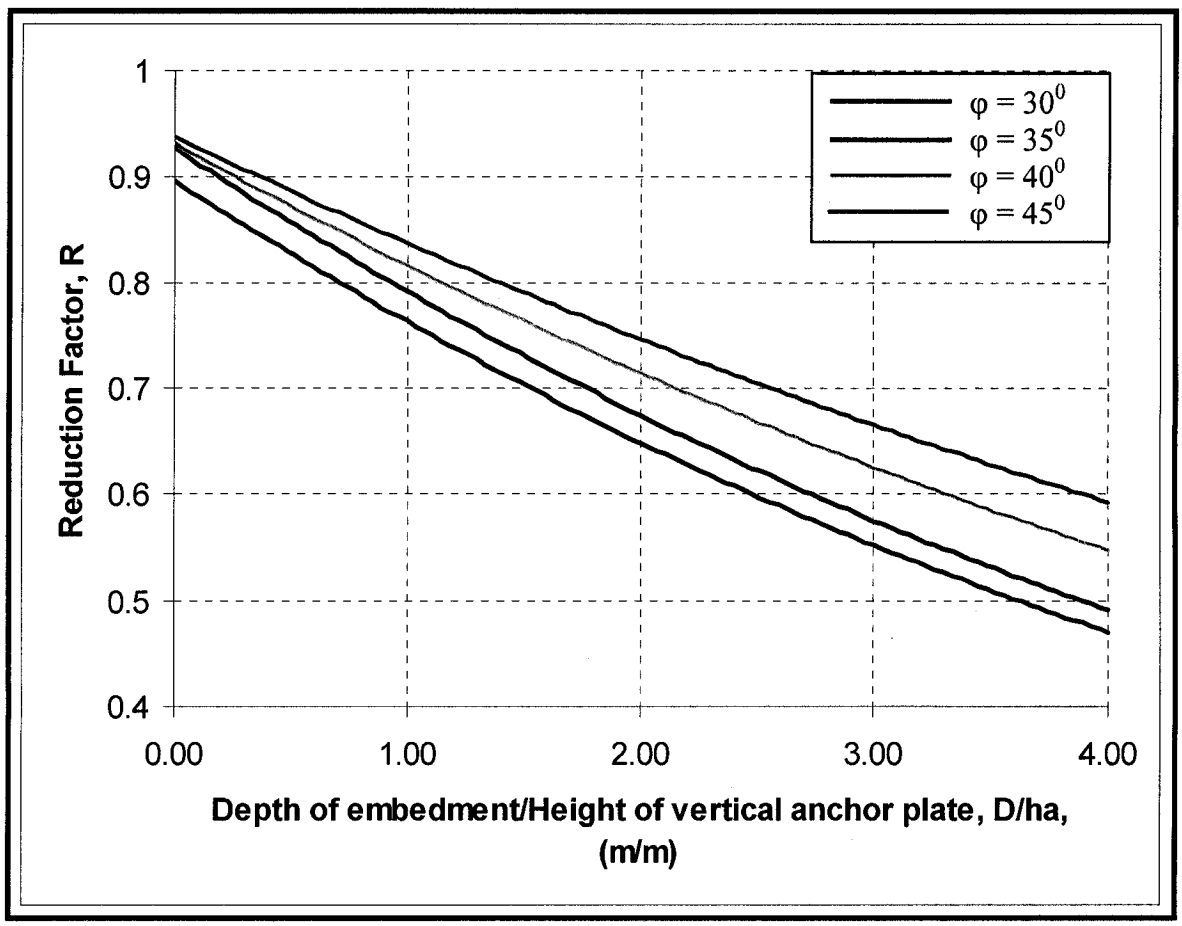

Figure 3.20 Proposed design charts for reduction factor, R at OCR=3

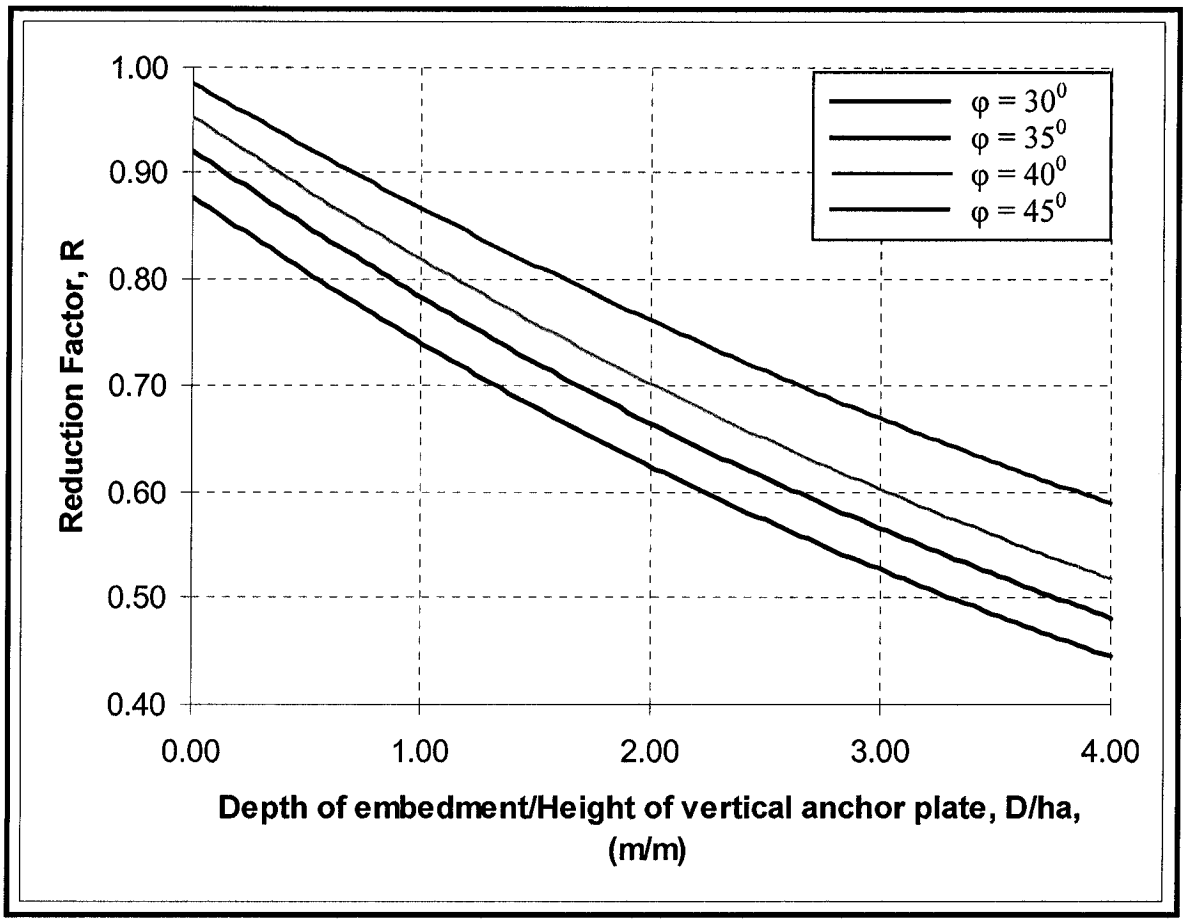

Figure 3.21 Proposed design charts for reduction factor, R at OCR=4

The angle of rotation, λ, can be determined in the following way.

A design chart, presented in figure 3.22, was proposed based on numerical analysis to calculate λ as a function of [D/h_a]. Here, the ultimate failure load, P_{ult} and K_p were obtained from numerical analysis and K_q was calculated using the equation,

$$K_q = \left[\frac{P_{ult} - \frac{1}{2} K_p \gamma H_{CG}^2}{\gamma D H_{CG}} \right] \qquad (3.24)$$

and,

$$\lambda = \cos^{-1}\left(\frac{K_p}{K_q} \right) \qquad (3.25)$$

Figure 3.22 presents a design chart for calculating λ at different ϕ, OCR and embedded depth.

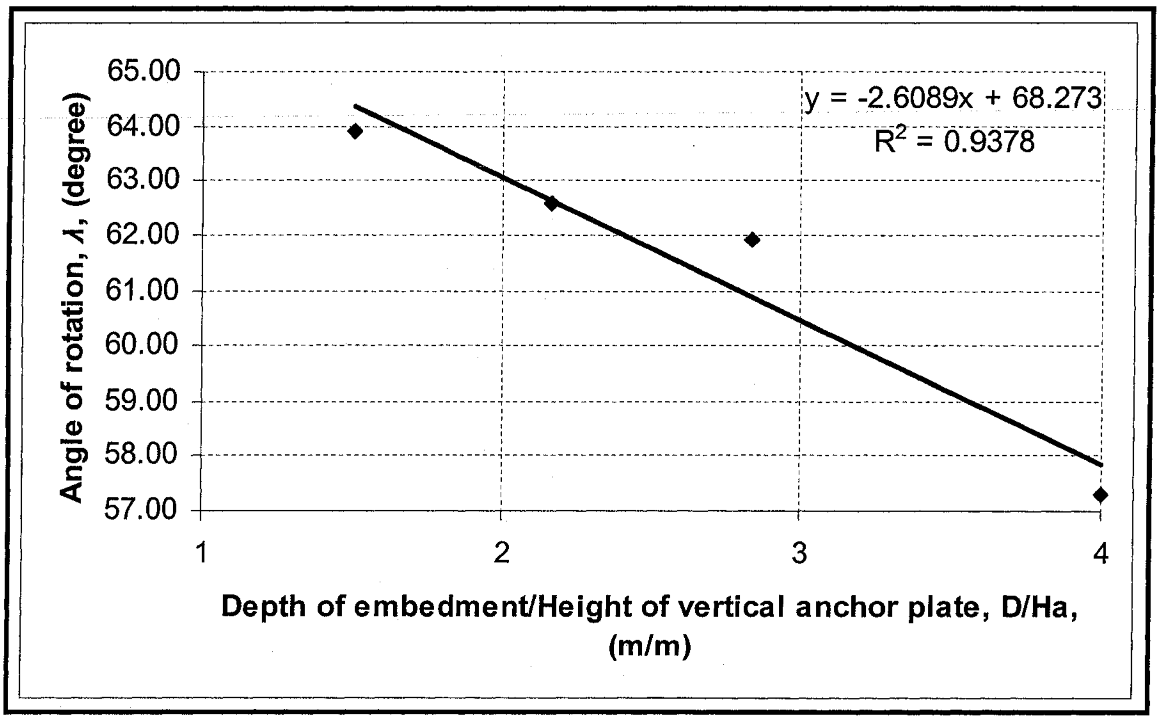

Figure 3.22 Rotational angle Vs depth/height ratio of vertical anchor plate

3.15.1.2 Mathematical Formulation for Load-Displacement Relation

The load-displacement relationship was proposed based on the method to calculate ultimate failure load used in numerical analysis. The load displacement curves obtained from the numerical model for different φ and OCR were not well able to locate the failure point and thus the Chin (1972) method was adopted to approximate the ultimate load at which the failure occurred.

Figure 3.23 shows the load-displacement curves obtained from numerical model and 3.24 describes the procedure how the ultimate load was calculated using Chin (1972) method.

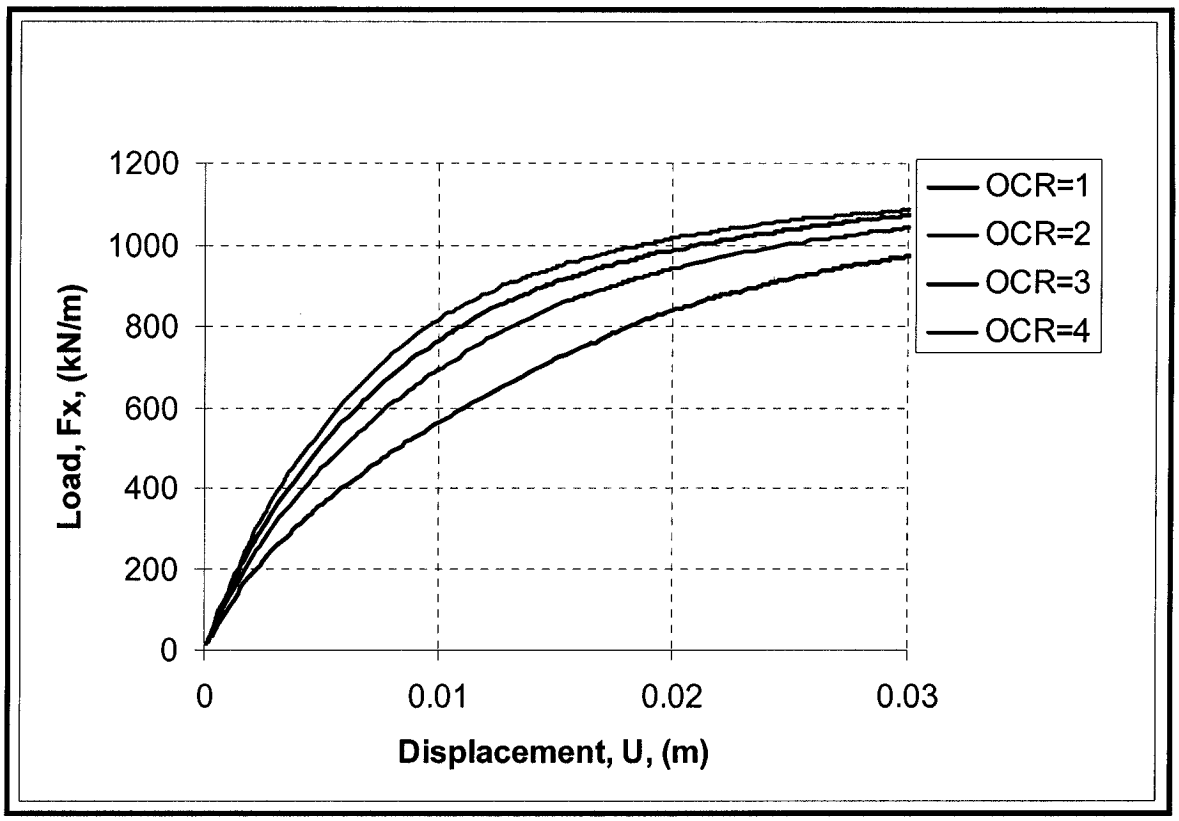

Figure 3.23 Load Vs Displacement curve in numerical model at φ = 45^0

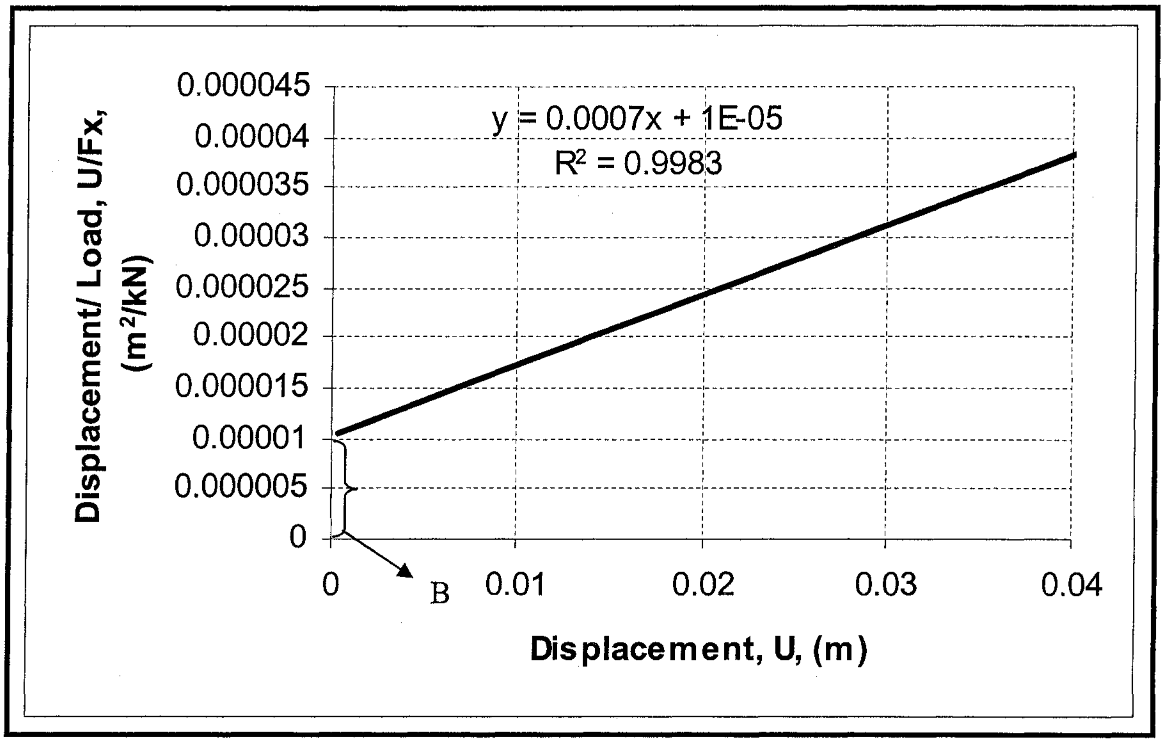

Figure 3.24 Calculation of ultimate load by Chin (1972) method at ϕ=45^0 and OCR=1

According to Chin (1972) method, inverse the slope of the curve (straight line) presented in figure 3.24 gives the ultimate or failure load at which the maximum passive state is reached. So the equation of the straight line can be written as:

$$\frac{U}{F_x} = \frac{1}{P_{ult}} \times U + B \quad \text{...(3.27)}$$

Here, U = applied displacement

F_x = load at displacement U

P_{ult} = failure load

B = constant (interception on Y axis) = f (ϕ, OCR)

Based on the equation of straight line presented in equation 3.27, the following mathematical load-displacement relationship was proposed to design the anchor under load-displacement relation. The ultimate load, P_{ult}, in the following equation was calculated using the equation 3.23 (section 3.15.1.1).

$$P = \left[\frac{\Delta}{\frac{\Delta}{P_{ult}} + B} \right] \quad \ldots \ldots \ldots \ldots \ldots \ldots \ldots \ldots \ldots \ldots \ldots \ldots \ldots \ldots \ldots \ldots \ldots (3.27)$$

Here, P = load at any admissible displacement

Δ = applied displacement

P_{ult} = the maximum failure load (calculated using equation 3.23)

B = interception on Y axis

The interception in Y axis, B is an arbitrary constant and is a function of ϕ and OCR. An empirical relation for B is also derived through the numerical model under different soil conditions. For different angle of shearing resistance, ϕ and OCR the following variation of B presented in figure 3.25 can be obtained from numerical model.

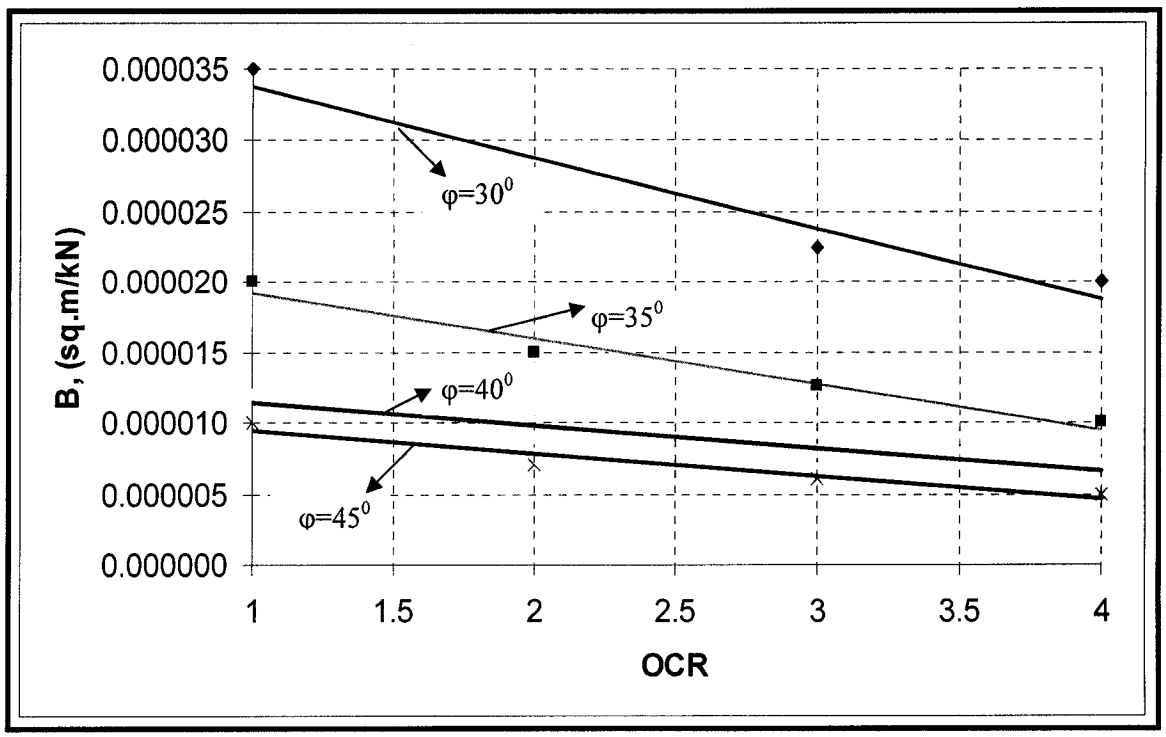

Figure 3.25 Variation of constant "B" with OCR at different φ

From the above figure 3.25, the equation of the straight line can be expressed as, $B = a_1 \times OCR + b_1$ where a_1 and b_1 are another two constants which are f (φ) only.

Figure 3.26 and 3.27 show the variation and equations for a_1 and b_1 with different angle of shearing resistance of soil, φ.

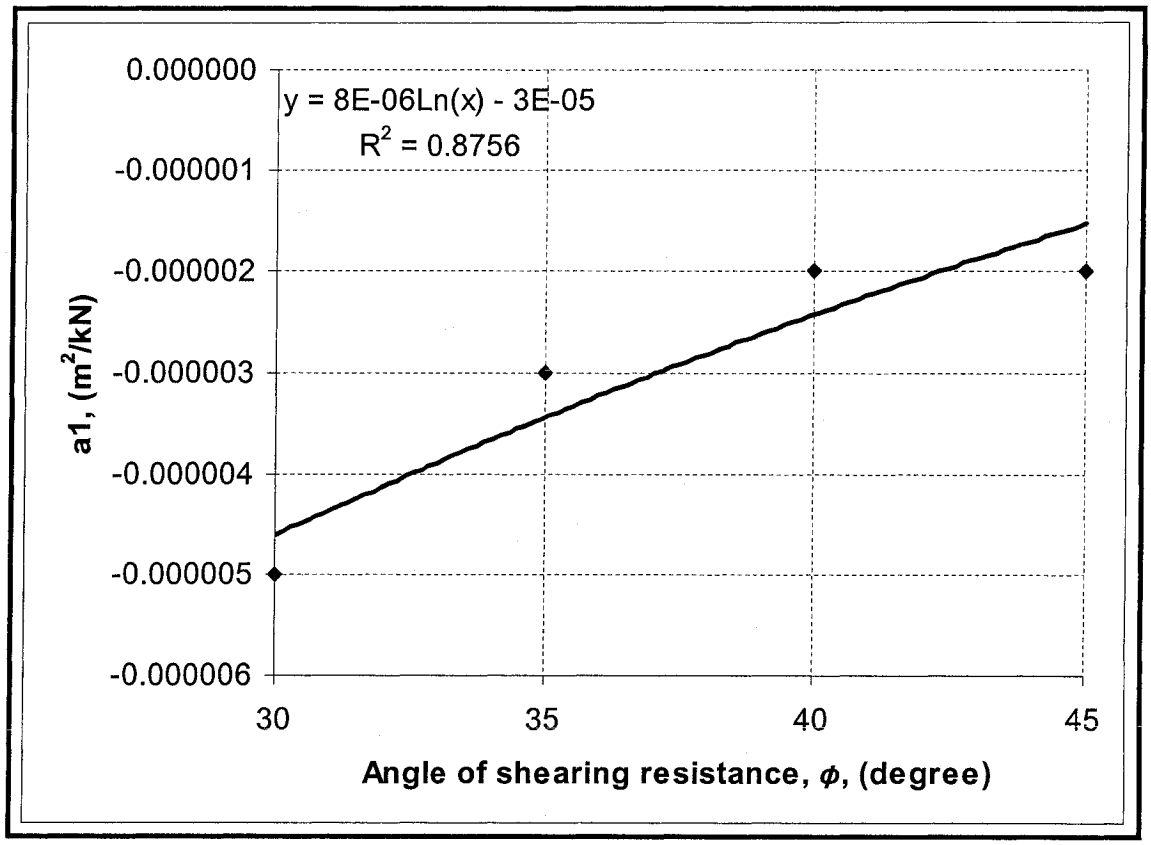

Figure 3.26 Variation of a_1 with ϕ in numerical model

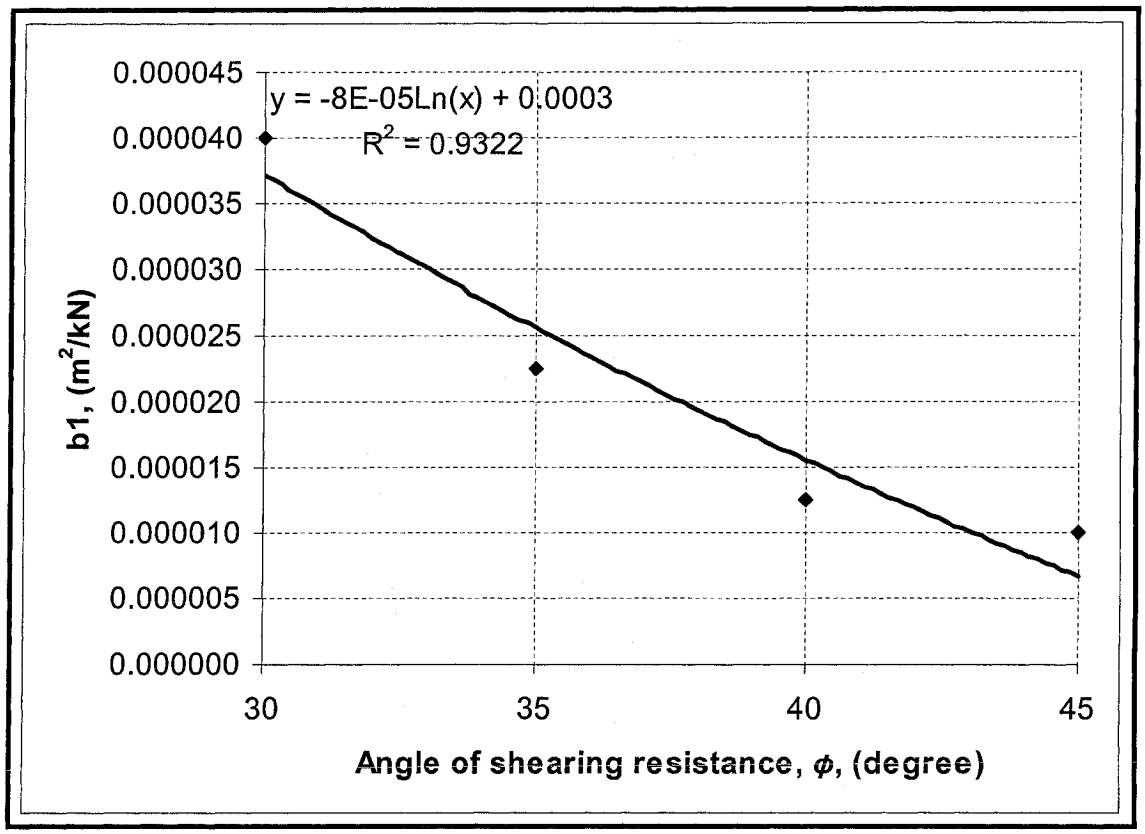

Figure-3.27: Variation of b_1 with ϕ in numerical model

From above two figures, the equations of a_1 and b_1 were derived as:

$$a_1 = 10^{-6}[8\ln\varphi - 30] \quad \ldots\ldots (3.27.1)$$

$$b_1 = 10^{-5}[-8\ln\varphi + 30] \quad \ldots\ldots (3.27.2)$$

Then, the equation of B can be stated as:

$$B = 10^{-6}[8\ln\varphi - 30][OCR - 10] \quad \ldots\ldots (3.27.3)$$

Finally, incorporating the value of B in equation 3.27, the expression for the load at any arbitrary displacement can be derived as:

$$P = \left[\frac{\Delta}{\frac{\Delta}{P_{ult}} + 10^{-6} \times [8\ln\varphi - 30][OCR - 10]}\right] \quad \ldots\ldots (3.28)$$

3.15.2 Comparison between proposed formula and numerical model

Comparison between the proposed formula and the numerical model are presented in figure 3.28, 3.29 and 3.30. This comparison was mainly based on the formulation presented in equation 3.28 and the load-displacement curves obtained from the numerical model with anchor plate.

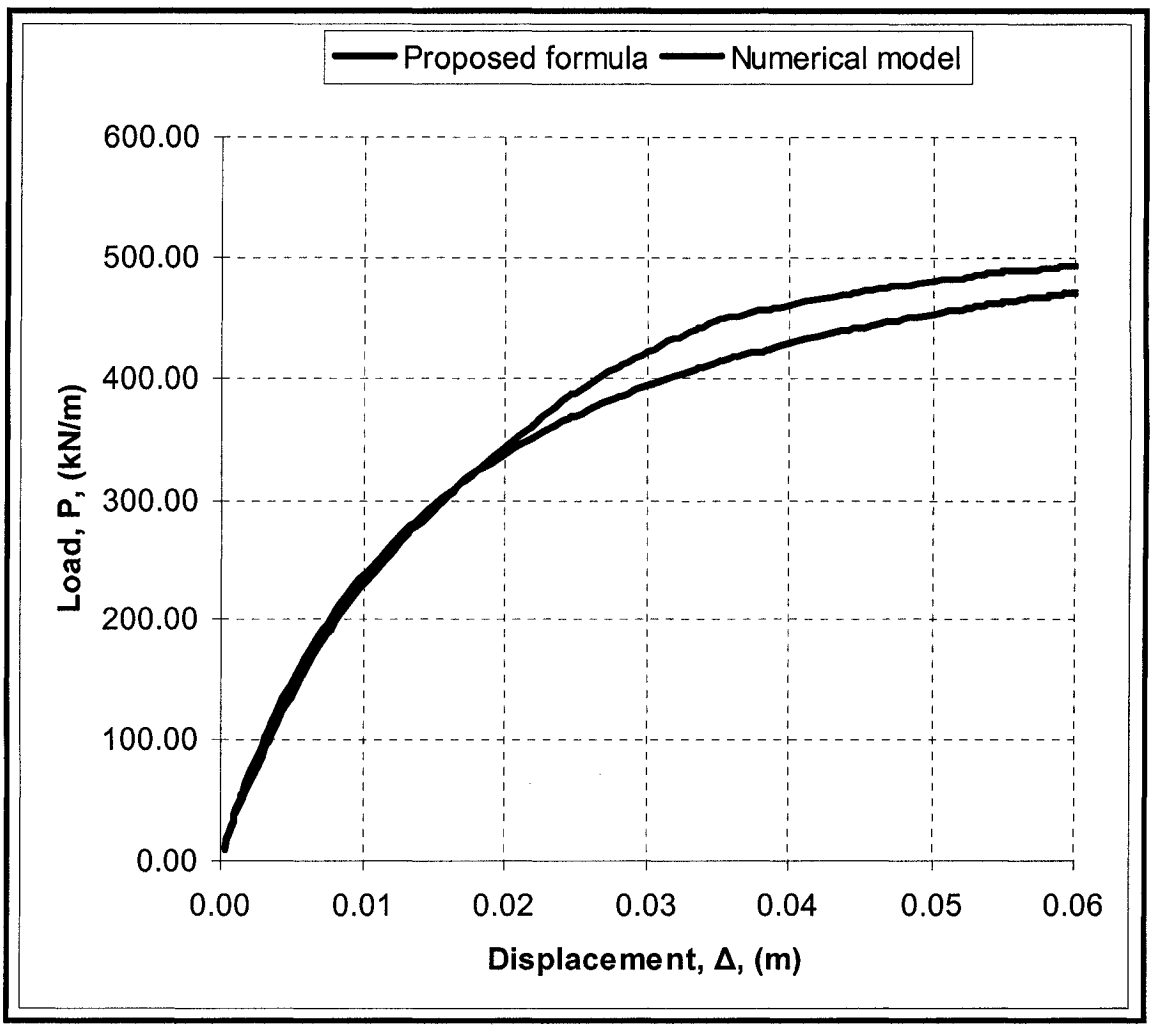

Figure 3.28 Load-displacement curve for OCR=2 and $\varphi = 30^0$

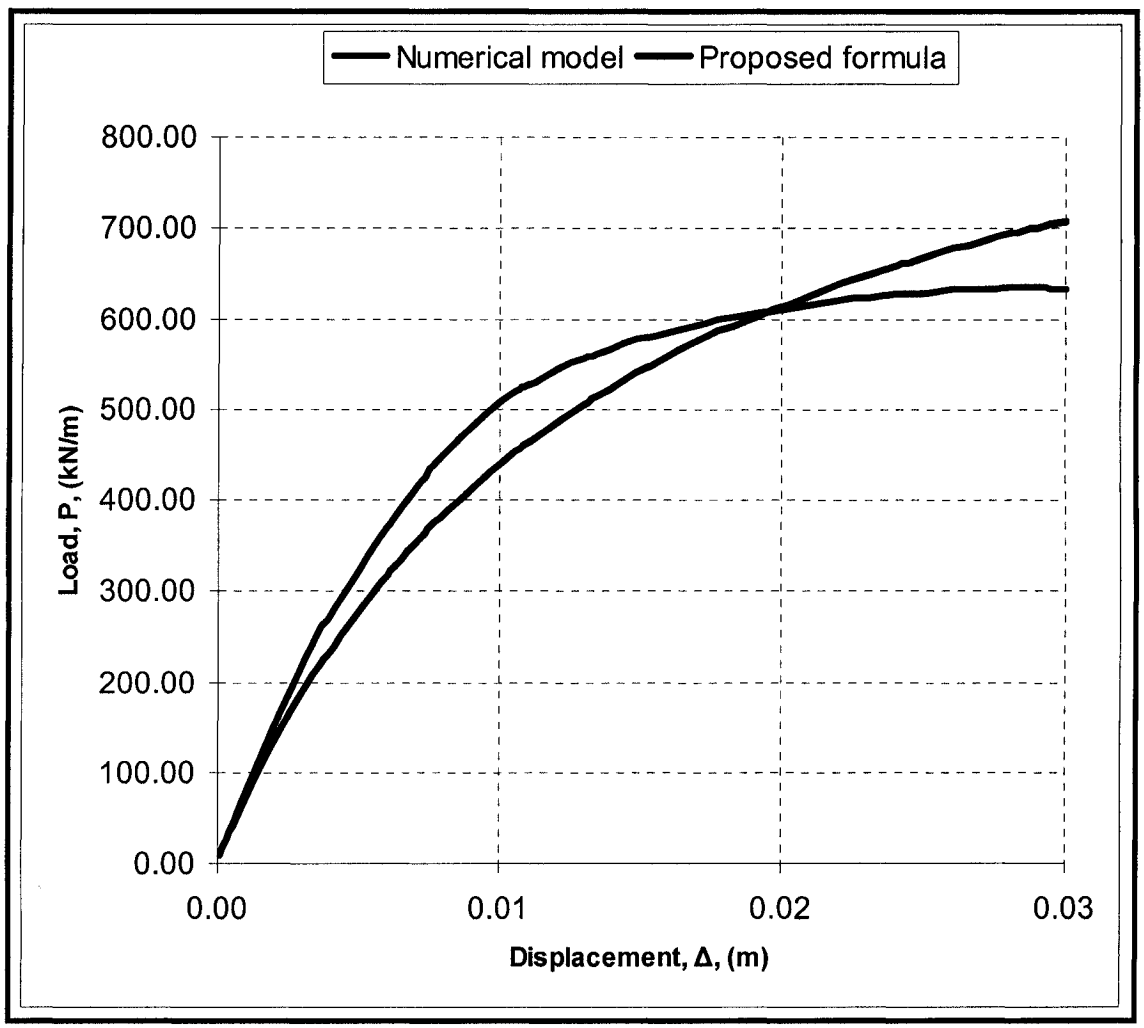

Figure 3.29 Load-displacement curve for OCR=3 and $\varphi = 35^0$

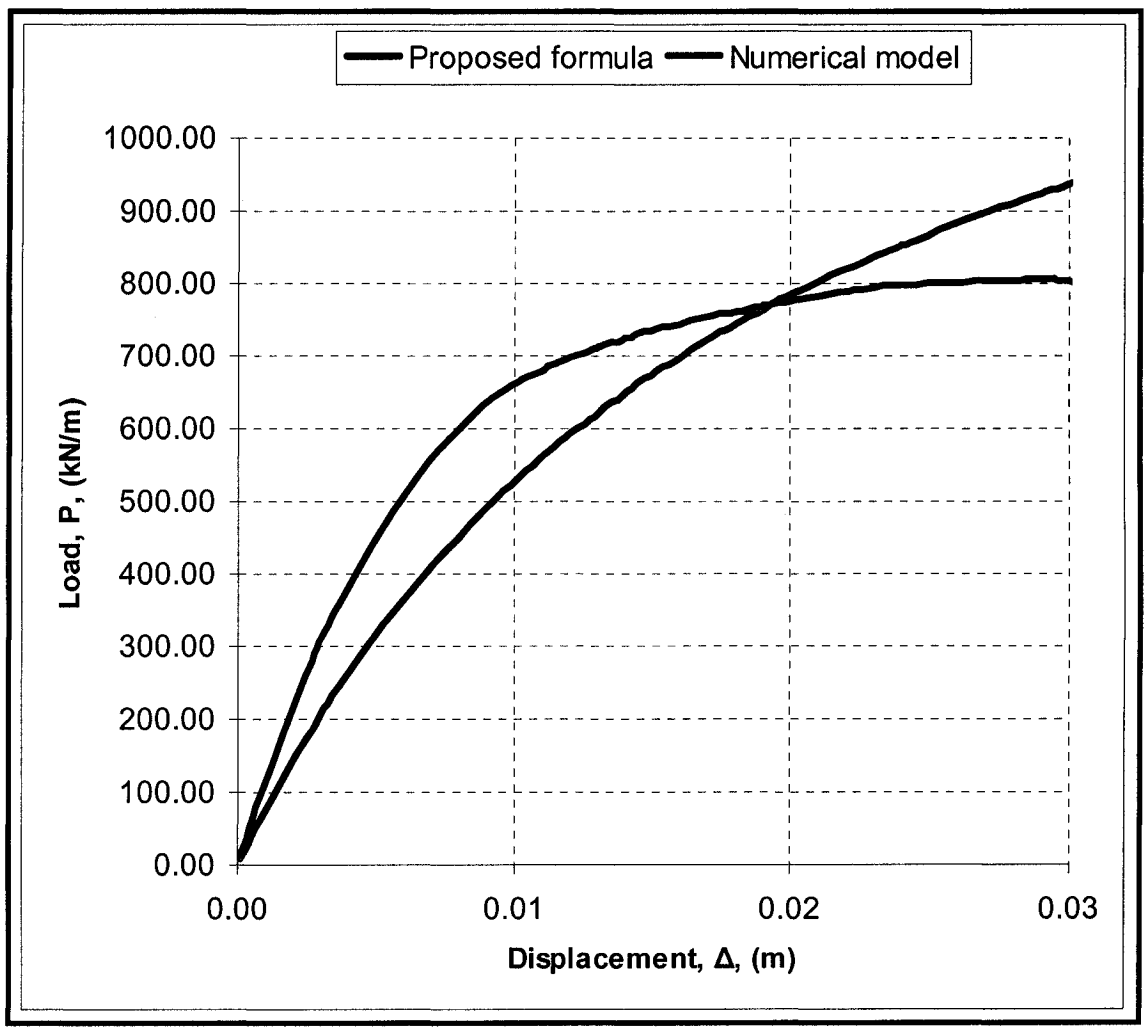

Figure 3.30 Load-displacement curve for OCR=4 and $\varphi = 40^0$

The agreement between the two results was quite satisfactory. From the above figures, it was found that with increasing ϕ and OCR, the discrepancy between the two results increases and it ranges from 1%-14% (<25%). It was mentioned previously that the Mohr-Coulomb model used in finite element analysis was less sensitive to OCR (section 3.12) and thus with higher OCR it provided a more conservative value compared to lower ϕ and OCR. So, it can be concluded that the proposed formulae presented in equation 3.23 and 3.28 will provide a reliable design (ultimate) load and the load-displacement relation to design an earth anchor.

3.15.3 Design Procedure for an Anchor Plate

Based on the numerical analysis developed in the present investigation, the following design procedure is suggested to design anchors embedded in a cohesionless backfill.

1. Locate the anchor plate in the ground, and accordingly the depth of excavation.

2. Select the dimensions of the anchor plate (height, width and thickness). The length of the anchor rod is determined by the equation 3.1 (section 3.3).

3. Determine the properties of the backfill materials. Determine the angle of shearing resistance, ϕ of the backfill material from the results of triaxial test.

4. Determine the OCR of the backfill.

5. Establish the eccentricity of the resultant of the earth pressure acting on the anchor plate (see figure 3.15) using figure 3.18 or equation 3.24.

6. Determine the location of the resultant earth pressure, H_{CG} can be calculated using equation 3.23.1.

7. Determine the rotation angle, λ, (table 3.17 and 3.18). For design purpose, λ can be determined using the proposed design chart presented in figure 3.22.

8. Determine the reduction factor using the design charts (figure 3.19, 3.20 and 3.21).

9. Calculate the values of coefficient of passive earth pressure, $K_{p(OC)}$ on anchor plate using equation 3.23.2.

10. Calculate the coefficient K_q using equation 3.23.3.

11. Estimation the failure load, P_{ult}, using equation. 3.23.

12. To design the anchor for a predetermined displacement, determine first the constant B using equation. 3.27.3. Then determine the load corresponding to that displacement using equation 3.28.

CHAPTER 4

CONCLUSIONS AND RECOMMENDATIONS

4.1 Conclusion

Geotechnical engineers are constantly searching for a safe and economical design for earth retention system to facilitate the construction of earth retaining walls. The anchor plate system is one of the most popular and suitable system for all type of soils.

During the last few years, several methods were proposed to investigate the earth pressure behind retaining walls, especially for those subjected to the passive condition. No attempts were made to measure the earth pressure acting on the anchor plate and accordingly the design of these plates remained un-established. Based on the results of the present investigation, the following can be concluded:

1. The passive earth pressure theories, which currently used to design anchor plate are grossly overestimate the design load on these anchors.
2. Numerical analysis is a powerful technique to solve soil-interaction problems as it overcomes the boundary effect that normally occurs in the small-scale laboratory experiment.
3. Stress history is a vital issue in determining the passive earth pressure.
4. The passive earth pressure in case of homogeneous overconsolidated backfill behind retaining walls increases with the increase of the angle of shearing resistance of the soil. For both homogeneous and layered soils, the theories

developed by Hanna and Khoury, 2005 to estimate the passive earth pressure on wall, is reconfirmed by the results of the present study.

5. Design procedure was developed in this study for the case of embedded anchor to incorporate the depth of embedment as an important governing parameter in estimating the value of K_p on the anchor plate.
6. Design theories are proposed to design the anchors for the two conditions; namely the ultimate load and the admissible displacement.

4.2 Future Recommendations

Based on the present investigation, the following is recommended for future research on the subject:

1. The present study should be extended to deal with the earth pressure on anchor plate subjected to rotation.
2. The theories developed in the present investigation should be validated with field data.
3. The case of anchor plate retains overconsolidated cohesionless soil overlying natural deposit should be investigated.

References

Anderson, W., Hanna, T. H. and Shan, S. A. (1977). "Model tests on anchored walls retaining overconsolidated sands." *Canadian Geotechnical Journal*, 14, 214-222

Baker, M. I. B (2003). "Passive earth pressure of overconsolidated cohesionless backfill overlying natural deposit." M.A.Sc thesis, Concordia University, Montreal

Broms, B. (1971). "Lateral earth pressure due to compaction of cohesionless soil." *Proceeding, fourth Budapest Conference on Soil Mechanics and Foundation Engineering, Budapest, Hungary,* 373-384

Brooker, E. W., and Ireland, H. O. (1965). "Earth pressure at rest related to stress history." *Canadian Geotechnical Journal,* 2(1), 1-15

Carder, D. R., Pocock, R. G. and Murray, R. T. (1977). "Experimental retaining wall facility-Lateral stress measurement with sand backfill." *Transportation and Road Research Laboratory Report,* LR 766

Caquot, A. and Kerisel, J. (1948), Table de poussee et butee, Gauthier-Vallars, Paris.

Chin, F. K. (1972). "The inverse slope as a prediction of ultimate bearing capacity of piles." *Proceedings of the 3rd Southeast Asian Conference on soil Engineering, Hong Kong,* 83-91

Clayton, C. R. I. and Symons, I. F. (1992). "The pressure of compacted fill on retaining wall." *Geotechmique,* 42(1), 127-130

Clemence, S. P., and Pepe, F. D. Jr., (1984). "Measurements of lateral stress around multi helix anchors in sand." *Geotechnical Testing Journal, ASTM,* 7(3), 145-152

Daramola, O. (1980). "On estimating K_o for over consolidated granular soil." *Geotechnique,* 30(3), 310-313

Diab, R. (1994). "Numerical Modeling of Passive Earth Pressure for normally and overconsolidated sands," M.A.Sc thesis, Concordia University, Montreal

Duncan, et al. (1991). "Estimation of earth pressure due to compaction." *Journal of Geotechnical Engineering, ASCE,* 117(12), 1833-1847

Duncan, J. M., Byrne, P., Wong, K. S., and Mabry, P. (1980). "Strength, stress-strain and bulk modulus parameters for finite element analysis of stresses and movements in soil masses." Department of Civil Engineering, University of California, Berkeley, Report No. UCB/GT/80-01

Duncan, J. M. and Seed, R. B. (1986). "Compaction induced lateral earth pressure under K_o conditions." *Journal of Geotechnical Engineering, ASCE,* 112(1), 1-22

Filz, G. M. and Duncan, J. M. (1996). "Earth pressure due to compaction: comparison of theory with laboratory and field behavior." *Transportation Research Record,* 1526, 28-37

Frydman, S. and Shaham, I. ((1989). "Pullout capacity of slab anchors in sand." *Canadian Geotechnical Journal*, 26, 385-400

Hanna, A. M and Ghaly, A. (1992). "Effect of K_o and overconsolidation on uplift capacity." *Journal of Geotechnical Engineering, ASCE*, 118(9), 1449-1469

Hanna, A. M. and Saad, N. S. (2001), "Effect of Compaction duration on the induced stress levels in a laboratory prepared sand bed." *Geotechnical Testing Journal, ASTM,* 24(4), 430-438

Hanna, A. M. and Khoury, I. A. (2005), "Passive earth pressure of overconsolidated cohesionless backfill," *Journal of Geotechnical and Geoenvironmental Engineering, ASCE*, 131(8), 978-986

Hua, Z. K. and Shen, C. K. (1987). "Lateral earth pressure on retaining structure with anchor plates." *Journal of Geotechnical engineering, ASCE*, 113(3), 189-201

Janbu, N. (1963), "Soil compressibility as determined by Oedometer and Triaxial tests." *European Conference on Soil Mechanism and Foundation Engineering, Wiesbaden, Germany,* 1, 19-25

Khoury, I. A. (1994), "Passive earth pressure behind a retaining wall for normally consolidated and overconsolidated cohesionless soil," M.A.Sc thesis, Concordia University, Montreal

Massarsch, R. K. and Fellenious, H. B. (2002). "Vibratory compaction of coarse-grained soil." *Canadian Geotechnical Journal,* 39, 695-709

PLAXIS MANUAL, 8.2, Professional Version. www.PLAXIS.com

Ranjan, G. and Kaushal, Y P (1977). "Load-displacement characteristics of model anchors under horizontal pull in sand." *Geotechnical Engineering*, 8, 65-78

Seed, R. B., (1983). "Soil structure interaction effects of compaction induced stresses and deformation." Doctoral thesis, University of California, Berkeley, USA

Seed, R. B. and Duncan, J. M., (1985). "FE analysis: Compaction induced stresses and deflections." *Journal of Geotechnical Engineering, ASCE,* 112(1), 23-43

Wang (2000). "Distribution of Earth Pressure on a Retaining Wall." *Geotechnique*, 50(1), 83-88

Wong, K. S. and Duncan, J. S. (1974). "Hyperbolic stress-strain parameters for nonlinear finite element analysis of stresses and movements in soil masses." Department of Civil engineering, University of California, Berkeley, Report TE-73-4

Worth (1975). "In-situ measurement of initial stresses and deformation characteristics." *Proceeding Specialty Conference on In-situ Measurement of Soil Properties*, *ASCE*, 1(2), 181-230